Control Design for Inhomogeneous-Broadening Compensation in Single-Photon Transducers

Sattwik Deb Mishra, Rahul Trivedi, Amir H. Safavi-Naeini, and Jelena Vučković

Phys. Rev. Applied **16**, 044025 — Published 14 October 2021

DOI: 10.1103/PhysRevApplied.16.044025

Control design for inhomogeneous-broadening compensation in single-photon transducers

Sattwik Deb Mishra*,[1] Rahul Trivedi*,[2] Amir H. Safavi-Naeini,[1] and Jelena Vučković[1]

[1] *Ginzton Laboratory, Stanford University, 348 Via Pueblo Mall, Stanford, California 94305, USA*
[2] *Max-Planck-Institute of Quantum Optics, Hans-Kopfermann-Str. 1, Garching 85748, Germany*

A transducer of single photons between microwave and optical frequencies can be used to realize quantum communication over optical fiber links between distant superconducting quantum computers. A promising scalable approach to constructing such a transducer is to use ensembles of quantum emitters interacting simultaneously with electromagnetic fields at optical and microwave frequencies. However, inhomogeneous broadening in the transition frequencies of the emitters can be detrimental to this collective action. In this article, we utilize a gradient-based optimization strategy to design the temporal shape of the laser field driving the transduction system to mitigate the effects of inhomogeneous broadening. We study the improvement of transduction efficiencies as a function of inhomogeneous broadening in different single-emitter cooperativity regimes and correlate it with a restoration of superradiance effects in the emitter ensembles. Furthermore, to assess the optimality of our pulse designs, we provide certifiable bounds on the design problem and compare them to the achieved performance.

INTRODUCTION

Current superconducting quantum systems are able to achieve non-trivial quantum computational tasks [1] and connecting them as nodes of a quantum internet can realize scalable, distributed quantum computing [2]. Since superconducting quantum systems operate at microwave frequencies, there are technological restrictions to directly connecting distant systems. Commercial microwave cables are dominated by thermal noise at room temperature and hence cause huge loss over long distances. On the other hand, cryo-cooled superconducting transmission lines are low loss but limited to short distances [3]. Optical photons are better 'flying' qubits; they can be transmitted with low loss over long distances through optical fibers. To connect superconducting quantum systems, there is a necessity to realize coherent transduction systems that can convert photons coherently and bi-directionally between microwave and optical frequencies.

Many approaches have been proposed to construct such transducers [4, 5]. Microwave-to-optical transducers couple fields oscillating at the respective frequencies through a non-linear medium that can be driven externally to bridge the gap between these frequency regimes. The different types of non-linear media that have been studied so far are, electro-optic materials [6–11], magnon modes [12–14], optomechanical systems [15–29], and broadly, ensembles of atomic systems [30–45].

Solid-state emitters (like color centers in diamond and silicon carbide and rare-earth ions doped in crystals) can have transitions coupling to both microwave and optical fields. They provide an attractive platform for implementing transducers owing to the possibility of integration with superconducting quantum systems [46, 47] and scalability afforded by rapidly developing nano-fabrication techniques [48–50]. However, single defects are often only weakly coupled to the microwave and optical fields, leading to low transduction efficiencies. An approach to overcoming this limitation is to use ensembles of such emitters coupling to the same microwave and optical channels the coupling strength is then enhanced proportionally to the number of emitters as a consequence of the formation of a collective superradiant state of the emitters [51–56].

In practical devices, emitters do not have identical resonant frequencies [57–59] this inhomogeneous broadening in the resonant frequencies prohibits the formation of a collective superradiant state and lowers the transduction efficiencies. However, the temporal shape of the lasers driving the emitter ensembles can be experimentally tuned — this opens up the possibility of using quantum control techniques to compensate for inhomogeneous broadening in the emitter ensemble, restore superradiance, and improve transduction efficiencies.

Quantum control techniques have traditionally been employed to control the state of quantum systems [60, 61] like ions [62, 63], atoms [64–66], superconducting qubits [67–69], and solid-state emitters [70, 71]. Furthermore, several previous works have also applied quantum control techniques for addressing inhomogeneous ensembles for various quantum technology applications. However, most of these previous results consider an inhomogeneous non-interacting ensemble, in which case the system can be effectively analyzed with the density matrix of a single emitter obtained by averaging the individual inhomogeneous emitter trajectories. Several results related to controllability of such systems have been previously provided [72–75], together with analytical [76–82] and numerical techniques [75, 83–97] to discover optimal controls. The problem of restoring superradiance in an inhomogeneous ensemble is distinct from the settings considered in these works in two key aspects — first, we must necessarily account for the collective interaction between the different

* These authors contributed equally to this work.

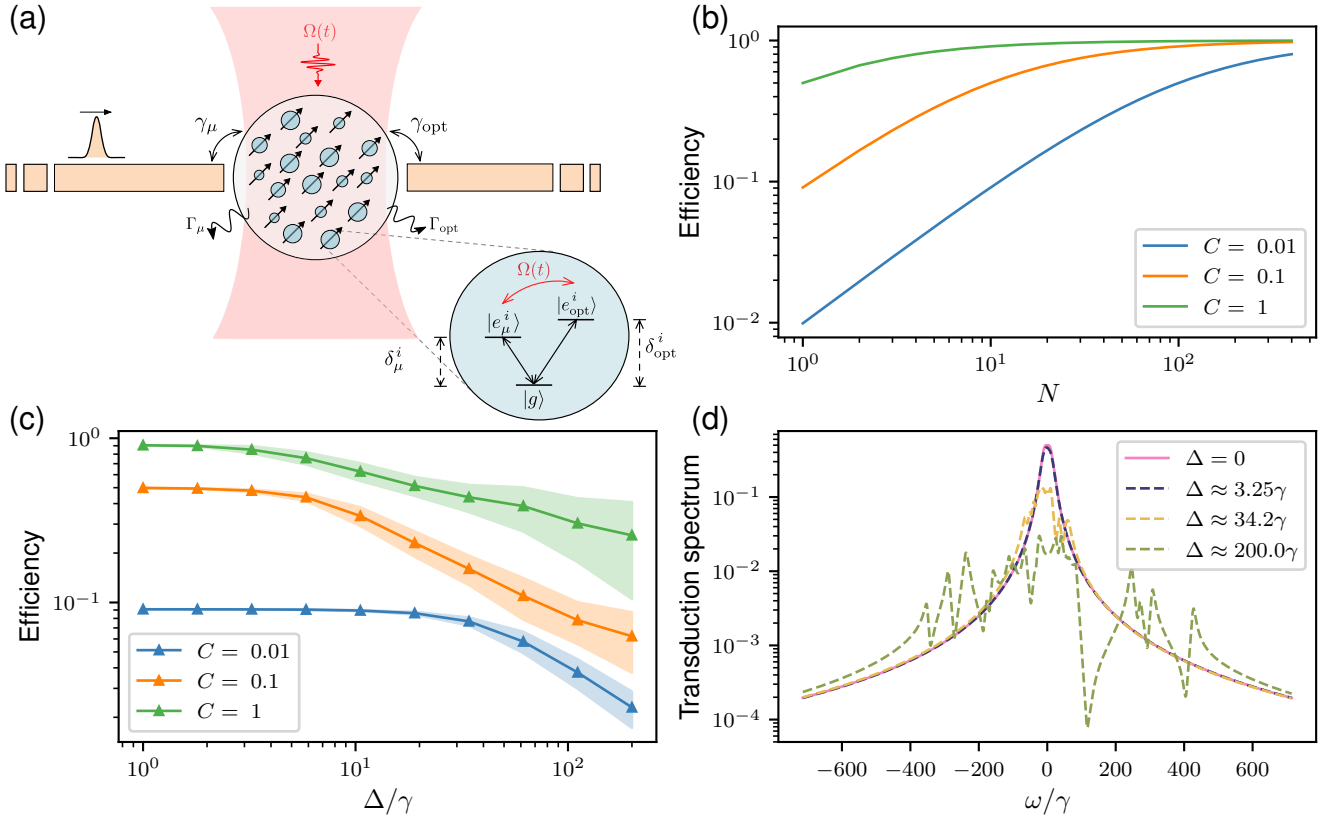

Figure 1. (a) Schematic of a three-level system ensemble-based transducer device. (b) Scaling of transduction efficiency with increasing number (N) of three-level systems in a homogeneous ensemble for different cooperativities C (we keep γ fixed and vary Γ to vary cooperativity). (c) Decrease in the transduction efficiency through randomly inhomogeneously broadened ensembles of $N = 10$ emitters with increasing inhomogeneous broadening Δ for different cooperativities C. For each value of the inhomogeneous broadening Δ, 100 randomly broadened ensembles are created by sampling the emitter detunings $\delta^{(i)}_\mu, \delta^{(i)}_{\rm opt}$ from a Gaussian distribution with standard deviation equal to Δ. Each plot point corresponds to the mean over the 100 ensembles with inhomogeneous broadening equal to the corresponding value of Δ and the shaded regions represent the standard deviation. (d) Transduction spectra of ensembles ($N = 10,\ C = 0.1$) with varying inhomogeneous broadening Δ.

emitters mediated by the optical and microwave fields by considering the state of the *entire* ensemble while designing the optimal control. Second, the model that we use is severely limited in terms of the control parameters available — we do not assume that each emitter is individually accessible as practical experimental setups can only easily apply a single control signal across all the emitters.

Our approach to solving this design problem is to use a time-dependent scattering theory framework [98] to pose the problem of inhomogeneity compensation as a control problem — this framework not only allows us to account for the collective interaction between the emitters as mediated by the optical and microwave fields, but also account for properties of the emitted and absorbed photons in the resulting quantum control problem. For the emitter based transduction system, we solve the resulting control problem using a gradient-based optimization algorithm to demonstrate an order of magnitude improvement in the transduction efficiencies. Furthermore, to assess the optimality of the resulting solution, we calculate provable upper bounds on the transduction efficiencies achievable by designing the temporal shape of the laser drive. Our work is closely related to, but distinct from Ref. [66] wherein a similar framework was used to design quantum controls for mediating interactions between ensembles of emitters with controllable transition frequencies to implement quantum memories.

RESULTS

The transducer model being considered in this article is schematically depicted in Fig. 1a. The emitter ensemble, with each emitter considered to be a three-level system, is coupled to microwave and optical modes with coupling

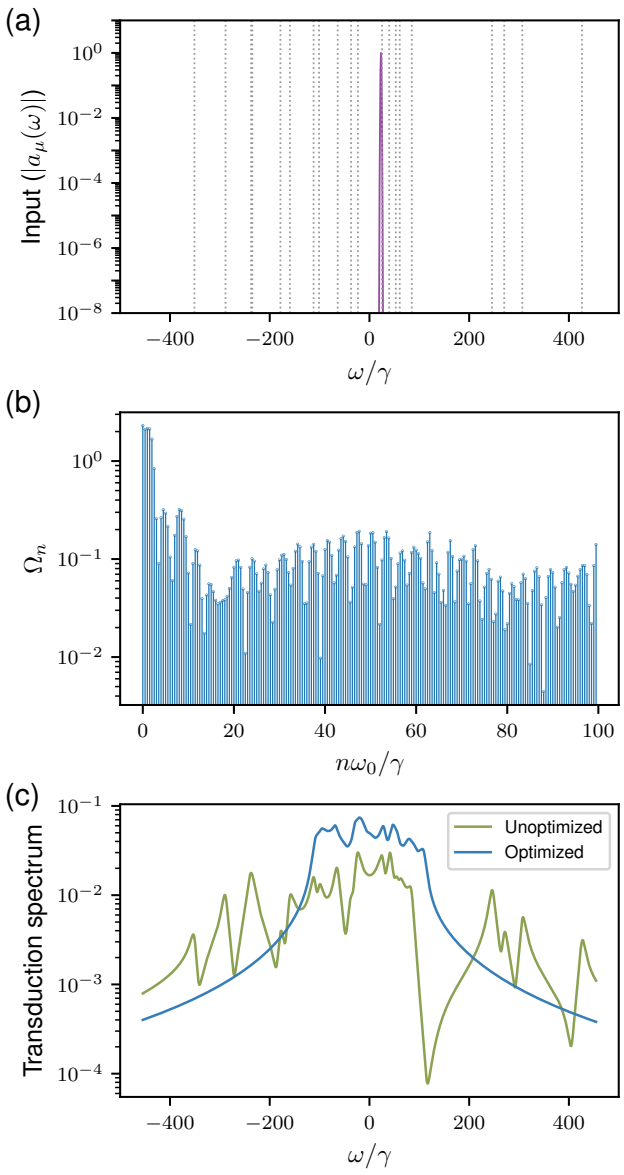

Figure 2. (a) Fourier transform of the input microwave field (Gaussian waveform). Dashed lines are representative of the individual emitter frequencies in a random ensemble ($N = 10$, $\Delta = 200\gamma$). (b) Amplitudes of the harmonic components of the optimized $\Omega(t)$ designed for the same ensemble. (c) Comparison of the transduction spectrum of the same ensemble with and without optimized drives applied — the transduction spectrum with the optimized drive is computed using a Floquet scattering theory approach [99].

operators L_μ and L_{opt} respectively, where

$$L_\mu = \sum_{i=1}^{N} \sqrt{\gamma_\mu}\sigma_\mu^i \text{ and } L_{\text{opt}} = \sum_{i=1}^{N} \sqrt{\gamma_{\text{opt}}}\sigma_{\text{opt}}^i. \quad (1)$$

Here, γ_μ and γ_{opt} are the decay rates of the emitters into the microwave and optical modes respectively, N is the number if emitters in the ensemble, and σ_μ^i and σ_{opt}^i are the lowering operators for transitions of the ith emitter in the ensemble. In addition to coupling to the optical and microwave modes, each emitter can also decay into additional loss channels, modeling unwanted radiative and non-radiative losses, with decay rates Γ_μ and Γ_{opt} from the excited states $|e_\mu^i\rangle$ and $|e_{\text{opt}}^i\rangle$, respectively. Furthermore, the transition between the two excited states is driven by a laser with envelope $\Omega(t)$.

For emitter ensembles formed out of identical emitters, the transduction efficiency is determined by the cooperativity of the individual transitions, $C_\mu = \gamma_\mu/\Gamma_\mu$ for microwave and $C_{\text{opt}} = \gamma_{\text{opt}}/\Gamma_{\text{opt}}$ for optical, as well as the number of emitters. We assume $\gamma_\mu = \gamma_{\text{opt}} = \gamma$, $\Gamma_\mu = \Gamma_{\text{opt}} = \Gamma$, and $C_\mu = C_{\text{opt}} = C = \gamma/\Gamma$ in our simulations for simplicity of analysis. Fig. 1b shows the transduction efficiency of this system as a function of the number of emitters for different emitter cooperativities due to the formation of a collective superradiant state between the different emitters, this efficiency asymptotically reaches 1 on increasing the number of emitters. Furthermore, the number of emitters needed to obtain high efficiency increases with a decrease in the cooperativity of the individual emitters. We point out that for high microwave and optical cooperativities, near unity transmissions can be obtained with a single emitter and consequently it is unnecessary to use emitter ensembles. We thus focus on low cooperativity emitters in the remainder of this article. On introducing inhomogeneous broadening into the emitter frequencies, the efficiency of the transduction system decreases (Fig. 1c) for large inhomogeneous broadening, the emitters do not form a collective superradiant mode and the transduction spectrum simply comprises of the individual transduction spectra of the emitters in the ensemble (Fig. 1d).

Since the laser pulse $\Omega(t)$ couples the microwave and optical transitions, we expect that unwanted variations in the transition frequencies can be compensated for by modulating the temporal form of this laser. However, in practical transduction systems, it is difficult to address individual emitters with separate lasers and consequently any modulation of $\Omega(t)$ impacts all the emitters. This makes designing the laser pulses difficult and calls for an application of numerical optimization techniques. We thus pose its design as maximizing the total power obtained in the optical mode when the emitter ensemble is excited with a single photon in the microwave mode:

$$\begin{aligned} \max_{\Omega(t)} \quad & \int_{-\infty}^{\infty} dt\ |a_{\text{opt}}(t)|^2 \\ \text{subject to} \quad & i\frac{d|\psi_e(t)\rangle}{dt} = H_{\text{eff}}(\Omega(t))\,|\psi_e(t)\rangle + a_\mu(t)L_\mu^\dagger|G\rangle, \\ & a_{\text{opt}}(t) = -i\langle G|L_{\text{opt}}|\psi_e(t)\rangle. \end{aligned} \quad (2)$$

where the time-domain wave-packets of the single microwave input photon and optical output photon are described by $a_\mu(t)$ and $a_{\text{opt}}(t)$ respectively, $|\psi_e\rangle$ is the state of the emitters in the ensemble, $|G\rangle$ is the ground state of the ensemble, and $H_{\text{eff}}(\Omega)$ is the non-Hermitian effective

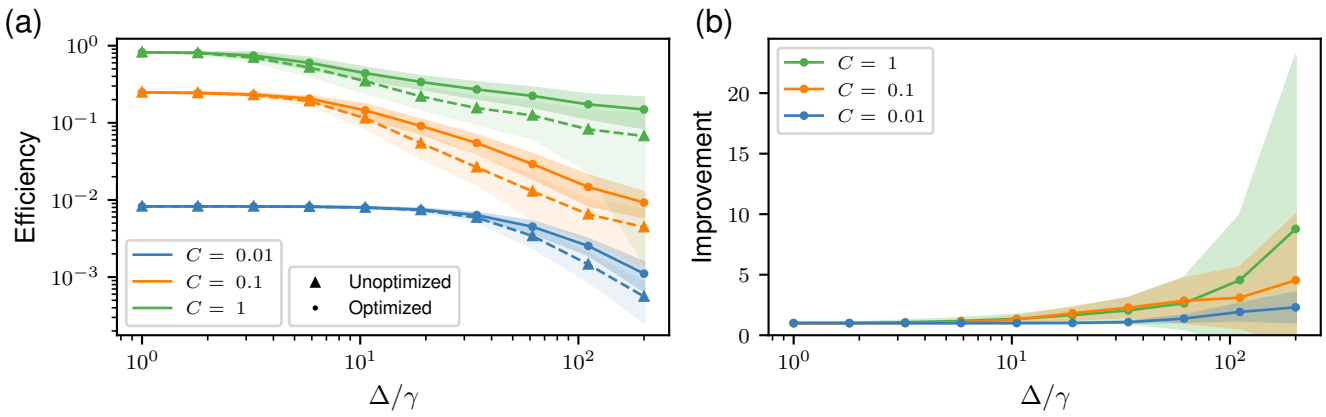

Figure 3. Optimized drives countering inhomogeneous broadening. (a) Transduction efficiency and (b) improvement in the transduction efficiency through randomly inhomogeneously broadened ensembles of $N = 10$ emitters with increasing inhomogeneous broadening for different cooperativities C when the optimized drives are applied. For each Δ, optimized drives are designed for each of the same 100 randomly generated ensembles with inhomogeneous broadening equal to Δ as used in Fig. 1c. Before running the optimizations, for each ensemble, the input photon is frequency-shifted to match the highest peak of the unoptimized transduction spectrum. Also, the initial condition for the optimization is $\Omega(t) = (N\gamma + \Gamma)/2$, which is a constant drive that maximizes the transduction efficiency through a homogeneous ensemble with the same decay rates (see Appendix C). Improvement is defined as the ratio of the efficiencies with and without the optimized drive applied. Each plot point corresponds to the mean over the 100 ensembles with inhomogeneous broadening equal to the corresponding value of Δ and the shaded regions represent the standard deviation.

Hamiltonian of the system when all the emitters are uniformly driven by a laser with amplitude Ω. We point out that the constraints are simply the input-output equations describing the dynamics of the transduction process under excitation with a single photon [98, 100, 101] — details of their derivation can be found in Appendix A. Furthermore, since experimentally realizable laser pulses will be band-limited, we parametrize $\Omega(t)$ as a finite sum of harmonics,

$$\Omega(t) = \sum_{n=0}^{N_h} \Omega_n \cos(n\omega_0 t + \phi_n), \tag{3}$$

consequently constraining its bandwidth to be $N_h\omega_0$. The design problem (2) can be solved using off-the-shelf gradient-based local optimizers. The gradient of the objective function in problem (2) with respect to the parameters Ω_n, ϕ_n can be computed using the time-domain adjoint variable method [102, 103] (details available in Appendix E).

As an example, we consider a transduction system with $N = 10$ inhomogeneous emitters excited with a single microwave photon with a Gaussian spectrum. Figure 2a shows the spectrum of the input photon, with the dashed lines depicting the resonant frequencies of the transduction spectra of the individual emitters. Given its narrow bandwidth, we expect the input photon to effectively only interact with a single emitter, leading to a low transduction efficiency comparable to what can be achieved by using just one emitter instead of many. The optimized drive obtained on solving problem (2) is depicted in Fig. 2b — as can be seen from Fig. 2c, the transduction spectrum in the presence of the optimized drive shows improvement relative to the one with constant (unoptimized) drive.

Statistical studies of performance of the optimization procedure for different sets of emitter frequencies is shown in Fig. 3 — Fig. 3a shows the optimized transduction efficiencies and Fig. 3b shows the improvement in the transduction efficiencies. We observe that the improvements are larger at higher inhomogeneous broadening. Furthermore, the cooperativities of the emitters set a limit on improvement that can be obtained by shaping the laser pulse — as can be seen from Fig. 3b, the improvements are generally smaller for lower cooperativities.

While it is intuitively expected that improvement in transduction efficiency with the application of an optimized drive is due to recovery of superradiance, this can be made more concrete by studying the Floquet eigenstates of the optimized (time-dependent) effective Hamiltonian. The superradiance in an eigenstate $|\phi\rangle$ of the propagator over one time period of the effective Hamiltonian, can be quantified with the metric,

$$f[|\phi\rangle] = \frac{2}{N\sqrt{\gamma_\mu \gamma_{\text{opt}}}} \left| \langle G|L_{\text{opt}}|\phi\rangle\langle\phi|L_\mu^\dagger|G\rangle \right|. \tag{4}$$

For a homogeneous ensemble, the metric is 1 for two eigenstates formed by the drive-induced hybridization of superradiant states corresponding to the microwave and optical transitions. Furthermore, it is 0 for the remaining eigenstates since they are subradiant/dark. Since the eigenstates for an inhomogeneous ensembles are not perfectly superradiant or subradiant, their corresponding

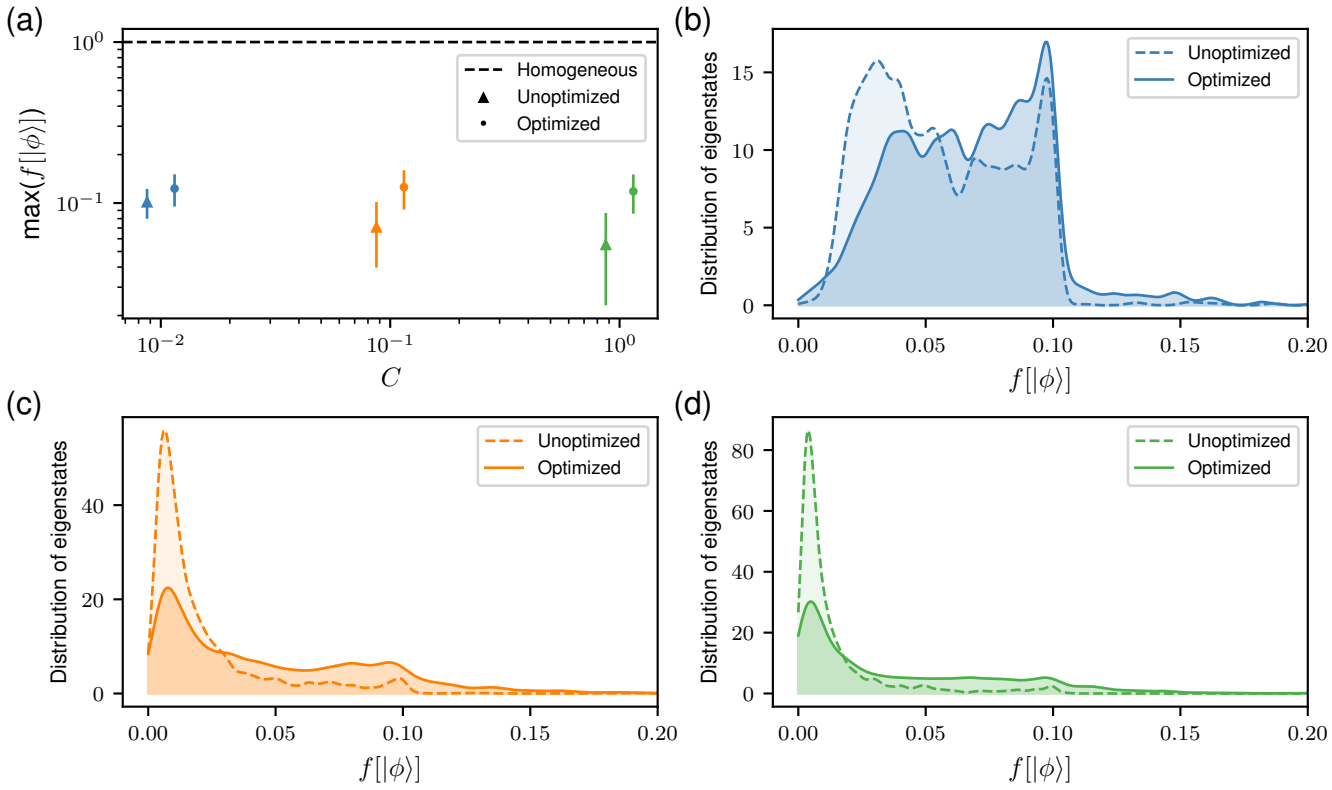

Figure 4. (a) Comparison of the superradiance metric for ensembles with inhomogeneous broadening $\Delta = 200\gamma$ with and without optimized drives applied (data for optimized and unoptimized cases are dodged in the plot for visual clarity). After generating the optimized drives used in Fig. 3, we compute the metric for all eigenstates of each of the 100 random ensembles with inhomogeneous broadening $\Delta = 200\gamma$ by numerically diagonalising the propagator over one time period of the effective Hamiltonian. Each plot point and associated error bars correspond to the mean and standard deviation (over the collection of ensembles with $\Delta = 200\gamma$) of the maximum value of the superradiance measure $f[|\phi\rangle]$ over all Floquet eigenstates $|\phi\rangle$. The dashed line denotes the same for a homogeneous ensemble. As we increase Γ to decrease the cooperativity, the metric is larger on average in the unoptimized case. We attribute this to the simultaneous increase in the unoptimized drive $\Omega(t) = (N\gamma + \Gamma)/2$ overshadowing the constant inhomogeneous broadening $\Delta = 200\gamma$ (see Appendix D). (b, c, d) Density plots (obtained by kernel density estimation using Gaussian kernels [104]) of the superradiance measure for eigenstates of the 100 ensembles with inhomogeneous broadening $\Delta = 200\gamma$, (b) $C = 0.01$, (c) $C = 0.1$, (d) $C = 1$.

metric lies between 0 and 1 and quantifies the extent of their subradiant or superradiant character. Figure 4a indicates that an application of the optimized drive statistically increases the value of this metric, indicating partial recovery of superradiance. The density plots in Fig. 4(b, c, d) show the distribution of the superradiance metric of the eigenstates of an inhomogeneously broadened ensemble.

The results discussed above indicate that pulse-shaping the laser can be used to improve the performance of transduction systems. However, the optimized laser pulses can only be computed if the emitter frequencies are known. For systems with large number of emitters, such characterization might not be practical at scale and it would be desirable to find an optimized pulse which is robust to the specific frequencies of the emitters and depends only on their distribution. To design such a laser pulse, we modify the optimization problem (2) to

$$\begin{aligned} \max_{\Omega(t)} \quad & \frac{1}{N_s}\sum_{n=1}^{N_s}\int_{-\infty}^{\infty} dt\, \left|a_{\text{opt}}^{(n)}(t)\right|^2 \\ \text{s.t.} \quad & i\frac{d|\psi_{\text{e}}^{(n)}(t)\rangle}{dt} = H_{\text{eff}}^{(n)}(\Omega(t))\,|\psi_{\text{e}}^{(n)}(t)\rangle + a_\mu(t)L_\mu^\dagger|G\rangle, \\ & a_{\text{opt}}^{(n)}(t) = -i\langle G|L_{\text{opt}}|\psi_{\text{e}}^{(n)}(t)\rangle, \end{aligned} \tag{5}$$

where we generate N_s inhomogeneous emitter samples from the same inhomogeneous broadening distribution and find a laser pulse that $\Omega(t)$ that optimizes the average transduced power over all the samples. The superscript over a quantity in problem (5) indicates that that quantity is computed for a specific sample. We design such a drive, shown in Fig. 5a, for a training set of $N_s = 100$ random ensembles with inhomogeneous broadening $\Delta = 200\gamma$ and with the input-photon being incident at the resonance of a homogeneous ensemble. Figure

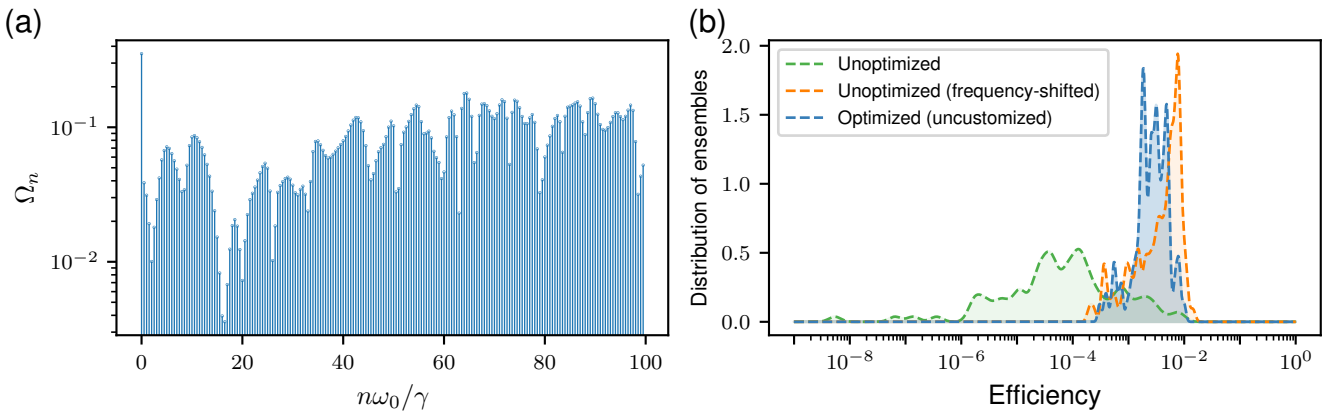

Figure 5. Transduction efficiency improvement with uncustomized optimization. (a) Amplitudes of the frequency components comprising the uncustomized drive. (b) Density plots of the transduction efficiency through 100 ensembles (test set) with $\Delta = 200\gamma$, $C = 0.1$ for three cases – (green) no optimized drive is applied and the input photon is fixed at the resonance of a homogeneous ensemble, (orange) no optimized drive is applied but the input photon is frequency-shifted to match the highest peak of the unoptimized transduction spectrum for each inhomogeneous ensemble, and (blue) the uncustomized optimized drive is applied and the input photon is fixed at the resonance of a homogeneous ensemble.

5b shows the resulting improvement in transduction efficiency from applying the optimized drive to a test set of 100 random ensembles that are generated from the same inhomogeneous broadening distribution, independently of the training set. While there is significant improvement over the unoptimized case, we point out that simply shifting the spectrum of the input photon without shaping the driving laser pulse results in similar improvements. Therefore, it is not expected that this optimized drive is restoring superradiance in the emitter ensemble, rather it is effectively matching the resonance of the transduction spectrum to the input photon in a manner robust to the specific emitter frequencies. This could still be technologically useful since this optimized drive is agnostic to the specific emitter frequencies, thus obviating the need to characterize the emitter resonances. Furthermore, if many transducers are to be operated simultaneously, experimentally realizing and supplying drives customized to each transducer can be challenging to scale — having a common, uncustomized drive would solve this problem.

Finally, we address the question about the optimality of the laser pulses calculated using the gradient-based optimization algorithm. Since the optimization problem (2) is non-convex, we can only solve it locally and calculating the solution globally will likely be hard. However, one method to assess how close the laser pulses obtained above are to the globally optimal solution is to calculate upper bounds on the achievable transduction efficiency and compare it to the locally optimized results.

The physically motivated idea behind calculating such an upper bound is to note that the efficiency is limited by the amplitude of the emitters in their excited state while interacting with the input photon, as well as the time that the emitters spend in the excited state. More rigorously, in the presence of the incident single-photon wave-packet as well as a decay of the excited state, the time-integrated norm of the excited state amplitude $|\psi_e(t)\rangle$ cannot be arbitrarily high. Consequently, an upper bound on the transduction efficiency can be obtained by simply maximizing the emitted photon energy as only constrained by this norm, which translates to solving the following optimization problem

$$\begin{aligned} \max_{\Omega(t)} \quad & \int_{-\infty}^{\infty} |a_{\text{opt}}(t)|^2 \, dt \\ \text{subject to} \quad & \int_{-\infty}^{\infty} \| |\psi_{\text{e}}(t)\rangle - |\psi_{\text{e},0}(t)\rangle \|_2^2 \, dt \leq \varepsilon \\ & a_{\text{opt}}(t) = -i\langle G|L_{\text{opt}}|\psi_{\text{e}}(t)\rangle, \end{aligned} \tag{6}$$

where $|\psi_{e,0}(t)\rangle$ is a reference state, $\|.\|_2$ denotes the l_2-norm, and ε is parameter that can be considered as the solution of the following optimization problem:

$$\begin{aligned} \max_{\Omega(t)} \quad & \int_{-\infty}^{\infty} \| |\psi_{\text{e}}(t)\rangle - |\psi_{\text{e},0}(t)\rangle \|_2^2 \, dt \\ \text{subject to} \quad & i\frac{d|\psi_{\text{e}}(t)\rangle}{dt} = H_{\text{eff}}(\Omega(t))\,|\psi_{\text{e}}(t)\rangle + a_\mu(t) L_\mu^\dagger |G\rangle. \end{aligned} \tag{7}$$

We point out that since by construction ε provides an upper bound on the integrated norm of the difference of the excited state from the reference state for all allowed laser pulses, the optimization problem 6 is a *relaxation* of the original non-convex optimization problem (problem 2). Therefore, the solution of problem 6 provides an upper bound to the (global) solution of problem 2.

Problem (6) is a quadratically-constrained quadratic program and bounds on its optimal value can be calculated by using the principle of Lagrangian duality

[105, 106] (see Appendix F). However, computing ε, which is required to solve problem 6, again requires solving a non-convex problem (problem 7). In order to get around this issue, as outlined in appendix F, we construct a provable upper bound, ε_c on ε which can also be used together with problem 6 to obtain an upper bound on the transduction efficiency. We point out that this bound will be looser than the one obtained on using ε, i.e., the tighter the bound on the norm of the excited state, the better the bound on the transduction efficiency.

Fig. 6 shows numerical studies of the upper bounds calculated on the transduction efficiency together with its comparison with the locally optimized results. In our numerical studies, we solve problem 6 to compute both a *certifiable* bound, which uses the upper bound ε_c on ε, and a *heuristic* bound calculated with only locally optimal solutions of problem 7. We observe that, as physically expected, the bounds decrease on average with increasing inhomogeneous broadening and are higher for higher cooperativities. Furthermore, the optimized transduction efficiencies are within an order of magnitude of the bound, which provides us with an estimate of the performance of the optimization method used in the paper.

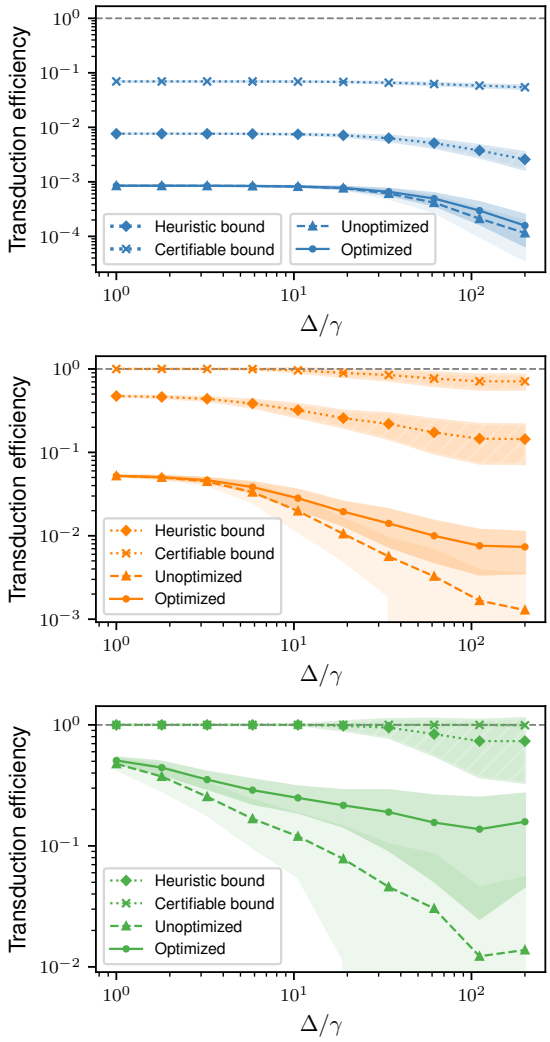

Figure 6. Heuristic and certifiable upper bounds and unoptimized and optimized transduction efficiencies calculated for ensembles with $N = 3$ emitters and cooperativities (a) $C = 0.01$, (b) $C = 0.1$, (c) $C = 1$. For each Δ, 100 random ensembles are generated with inhomogeneous broadening equal to Δ. For each such ensemble, optimized drives are designed to improve transduction efficiency by using a local optimizer to solve problem (2). Then, using the state obtained by solving the input-output equation with the aforementioned optimized drive as the reference state, heuristic and certifiable bounds are calculated. Each plot point corresponds to the mean over the 100 ensembles with inhomogeneous broadening equal to the corresponding value of Δ and the shaded regions represent the standard deviation.

DISCUSSION

In this article, we have used gradient-based inverse design of the temporal shape of the driving field as a technique to compensate for the effects of inhomogeneous broadening to help realize more efficient transducers. We demonstrated that optimized driving fields can lead to improvement in transduction efficiencies and showed that this improvement can be correlated with restoration of superradiant effects. Finally, to characterize the limits of the performance of time-dependent drives obtained by optimization-based design, we calculated upper bounds on optimal transduction efficiencies.

Our design method is applicable to different physical platforms including color centers or rare-earth ions in solid-state hosts. The techniques used in this article can be extended to ensembles that are orders of magnitude larger by frequency-binning the randomly distributed transition frequencies [107]. We will explore this direction in future work. In some physical systems the transition frequencies of the emitters can be modulated (for e.g., via Stark effect in V_{Si} centers in SiC). Previous research [108] has shown that direct modulation of the transition frequencies can also be used to compensate for inhomogeneous broadening in a cavity-QED setting. We anticipate that optimization-based design for transducers can also be applied with the direct modulation as the degree of freedom instead of the driving field.

Regarding experimental implementation of our design method, pulse shaping of the laser drive should be achievable by using a commercial electro-optic intensity modulator — we assume in our simulations that the highest harmonic component in the drive has a frequency of 1 GHz ($\gamma = 10$ MHz). The experimental feasibility of designing photon emission and scattering properties by time-modulating solid-state emitters has been demonstrated before [108–110], albeit with modulation methods different from a laser drive.

METHODS

Simulations

We discretize the input-output equations (the constraints in problem (2)) in time and simulate the dynamics to calculate the transduction efficiency using finite-difference methods. For the customized case, i.e., when the drive is designed for a specific ensemble, we use the L-BFGS-B optimization algorithm. We employ the stochastic optimization algorithm *Adam* [111] to design the uncustomized driving field.

ACKNOWLEDGEMENTS

The authors thank Shuo Sun, Logan Su, Hubert Stokowski, and Kevin Karan Singh Multani for useful discussions. This research is funded in part by the U.S. Department of Energy, Office of Science, under Awards DE-SC0019174 and DE-Ac02-76SF00515. R.T. acknowledges funding from Kailath Graduate Fellowship.

S.D.M. and R.T. contributed equally to this work. R.T. and J.V. conceived the idea of using optimization-based design of drives for inhomogeneous broadening compensation. R.T., S.D.M., and A.H.S.-N. designed the numerical experiments. S.D.M. and R.T. performed the numerical and theoretical analysis. All authors wrote the manuscript.

Appendix A: Input-output equations

The Hamiltonian describing the ensemble is,

$$H_{\rm sys}(\Omega(t)) = \sum_i \left[\delta^i_\mu \sigma^{i\dagger}_\mu \sigma^i_\mu + \delta^i_{\rm opt}\sigma^{i\dagger}_{\rm opt}\sigma^i_{\rm opt}\right] + \sum_i \Omega(t)(\sigma^{i\dagger}_\mu \sigma^i_{\rm opt} + \text{H. c.}), \tag{A1}$$

where the transition operators $\sigma^i_{\mu,\rm opt}$ are defined in the main text. We point out that the laser field is actually $\Omega\left(t\right)e^{i\omega_L t}$, where ω_L is the central frequency. The Hamiltonian in Eq. A1 is obtained by going into a rotating frame to remove the term oscillating at ω_L from the drive.

The Hamiltonian of the entire system, i.e., the microwave and optical waveguide modes together with the ensemble is,

$$H = -i\int dx\ \left(a^\dagger_{\mu,x}\frac{\partial}{\partial x}a_{\mu,x} + a^\dagger_{{\rm opt},x}\frac{\partial}{\partial x}a_{{\rm opt},x}\right) + \left(a^\dagger_{\mu,x=0}L_\mu + \text{H.c.}\right) + \left(a^\dagger_{{\rm opt},x=0}L_{\rm opt} + \text{H.c.}\right) + H_{\rm sys}, \tag{A2}$$

where $a_{\mu,x}$ and $a_{{\rm opt},x}$ are the spatial annihilation operators for the microwave and optical waveguide modes respectively [98] and the coupling operators L_μ and $L_{\rm opt}$ are defined in the main text. The terms in Eq. A2 with the operators L_s where $s \in \{\mu, {\rm opt}\}$ represent the ensemble-waveguide interaction.

We define the number operator,

$$N_e = \int dx\ \left(a^\dagger_{\mu,x}a_{\mu,x} + a^\dagger_{{\rm opt},x}a_{{\rm opt},x}\right) + \sum_{i=1}^{N}\left(\sigma^{i\dagger}_\mu\sigma^i_\mu + \sigma^{i\dagger}_{\rm opt}\sigma^i_{\rm opt}\right), \tag{A3}$$

which commutes with the Hamiltonian H. We consider an initial state with a single photon in the microwave waveguide mode. Thus, the state of the whole system is restricted to the single-excitation subspace at all times, and we assume the following ansatz for the state at time t in the Schrödinger picture,

$$|\psi\left(t\right)\rangle = \int dx\ \alpha\left(x,t\right)a^\dagger_{\mu,x}|\text{vac}\rangle\otimes|G\rangle\otimes|\text{vac}\rangle + |\text{vac}\rangle\otimes|\psi_e\left(t\right)\rangle\otimes|\text{vac}\rangle + |\text{vac}\rangle\otimes|G\rangle\otimes\int dx\ \beta\left(x,t\right)a^\dagger_{{\rm opt},x}|\text{vac}\rangle, \tag{A4}$$

where $|\text{vac}\rangle$ is the vacuum state of a waveguide mode and $|G\rangle = \bigotimes_{i=1}^{N}|g\rangle$ is the ground state of the ensemble.

Given this ansatz, Schrödinger's equations for the system are,

$$i\frac{d}{dt}|\psi_e\left(t\right)\rangle = H_{\rm sys}|\psi_e\left(t\right)\rangle + \alpha\left(0,t\right)L^\dagger_\mu|G\rangle + \beta\left(0,t\right)L^\dagger_{\rm opt}|G\rangle \tag{A5}$$

$$\frac{\partial}{\partial t}\alpha\left(x,t\right) = -\frac{\partial}{\partial x}\alpha\left(x,t\right) - i\delta\left(x\right)\langle G|L_\mu|\psi_e\left(t\right)\rangle \tag{A6}$$

$$\frac{\partial}{\partial t}\beta\left(x,t\right) = -\frac{\partial}{\partial x}\beta\left(x,t\right) - i\delta\left(x\right)\langle G|L_{\rm opt}|\psi_e\left(t\right)\rangle, \tag{A7}$$

Solving Eq. A6 and Eq. A7 for $\alpha\left(0,t\right)$ and $\beta\left(0,t\right)$,

$$\alpha(0,t) = a_\mu(t) - \frac{i}{2}\langle G|L_\mu|\psi_e(t)\rangle \tag{A8}$$

$$\beta(0,t) = -\frac{i}{2}\langle G|L_{\rm opt}|\psi_e(t)\rangle, \tag{A9}$$

where $a_\mu\left(t\right) = \lim_{t_0\to-\infty}\alpha\left(t_0 - t, t_0\right)$ describes the time-domain wave-packet of the input photon in the microwave waveguide mode. Similarly, $a_{\rm opt}\left(t\right) = \lim_{t_1\to\infty}\beta\left(t_1 - t, t_1\right)$ describes the time-domain wave-packet of the output photon in the optical waveguide mode. From the solution of Eq. A7 we have,

$$a_{\rm opt}(t) = -i\langle G|L_{\rm opt}|\psi_e(t)\rangle. \tag{A10}$$

Substituting Eq. A8 and Eq.A9 into Eq. A5, we have,

$$i\frac{d}{dt}|\psi_e\left(t\right)\rangle = \left(H_{\rm sys} - \frac{i}{2}L^\dagger_\mu|G\rangle\langle G|L_\mu - \frac{i}{2}L^\dagger_{\rm opt}|G\rangle\langle G|L_{\rm opt}\right)|\psi_e\left(t\right)\rangle + a_\mu(t)L^\dagger_\mu|G\rangle. \tag{A11}$$

We point out that $L_s^\dagger L_s = L_s^\dagger \left(P_e + |G\rangle\langle G|\right) L_s = L_s^\dagger |G\rangle\langle G| L_s$ where $s \in \{\mu, \text{opt}\}$ and P_e is the projector onto the excited state space spanned by $\{|e_\mu^i\rangle, |e_{\text{opt}}^i\rangle : i \in \{1, \ldots, N\}\}$. Thus, Eq. A11 can be rewritten as,

$$i\frac{d}{dt}|\psi_e(t)\rangle = \left(H_{\text{sys}} - \frac{i}{2}L_\mu^\dagger L_\mu - \frac{i}{2}L_{\text{opt}}^\dagger L_{\text{opt}}\right)|\psi_e(t)\rangle + a_\mu(t)L_\mu^\dagger|G\rangle. \tag{A12}$$

Furthermore, the decays from the excited states of the emitters into various loss channels besides the waveguides can be captured in a similar manner by adding terms like $-\frac{i\Gamma_s^i}{2}\sigma_s^{i\dagger}\sigma_s^i|\psi_e(t)\rangle$ where $s \in \{\mu, \text{opt}\}$ to the right side of Eq. A12. Then we have,

$$i\frac{d}{dt}|\psi_e(t)\rangle = H_{\text{eff}}(\Omega(t))|\psi_e(t)\rangle + a_\mu(t)L_\mu^\dagger|G\rangle, \tag{A13}$$

where,

$$H_{\text{eff}}(\Omega(t)) = \left(H_{\text{sys}}(\Omega(t)) - \sum_i \left(\frac{i\Gamma_\mu}{2}\sigma_\mu^{i\dagger}\sigma_\mu^i - \frac{i\Gamma_{\text{opt}}}{2}\sigma_{\text{opt}}^{i\dagger}\sigma_{\text{opt}}^i\right) - \frac{i}{2}L_\mu^\dagger L_\mu - \frac{i}{2}L_{\text{opt}}^\dagger L_{\text{opt}}\right). \tag{A14}$$

Eq. A13 and Eq. A10 (upto a phase factor of i) are the input-output equations used in our simulations.

Appendix B: Inhomogeneous broadening and transduction efficiency

We study how collective action of the emitters can be used to boost the effective cooperativity. For a homogeneous ensemble of size N, we define the operator-valued vectors,

$$\Sigma_\mu = \begin{pmatrix}\sigma_\mu^1\\ \vdots \\ \sigma_\mu^N\end{pmatrix}, \Sigma_{\text{opt}} = \begin{pmatrix}\sigma_{\text{opt}}^1\\ \vdots \\ \sigma_{\text{opt}}^N\end{pmatrix}.$$

Next, we consider a change of basis through the action of a $N \times N$ unitary matrix V on the vectors defined above.

$$\begin{aligned} S_\mu &= V\Sigma_\mu = \left(S_{\mu,1},\ \ldots,\ S_{\mu,N}\right)^T \\ S_{\text{opt}} &= V\Sigma_{\text{opt}} = \left(S_{\text{opt},1},\ \ldots,\ S_{\text{opt},N}\right)^T. \end{aligned} \tag{B1}$$

The transformation V is defined such that

$$\begin{aligned} S_{\mu,1} &= \frac{1}{\sqrt{N}}\sum_{i=1}^N \sigma_\mu^i \\ S_{\text{opt},1} &= \frac{1}{\sqrt{N}}\sum_{i=1}^N \sigma_{\text{opt}}^i. \end{aligned} \tag{B2}$$

After the transformation, and assuming that $\gamma_\mu = \gamma_{\text{opt}} = \gamma,\ \Gamma_\mu = \Gamma_{\text{opt}} = \Gamma$, the effective Hamiltonian becomes,

$$\begin{aligned} H_{\text{eff}} = &\left[\left(\delta_\mu - \frac{i\Gamma}{2}\right)S_\mu^\dagger S_\mu + \left(\delta_{\text{opt}} - \frac{i\Gamma}{2}\right)S_{\text{opt}}^\dagger S_{\text{opt}}\right] \\ &+ \Omega(S_\mu^\dagger S_{\text{opt}} + \text{H. c.}) - \frac{iN\gamma}{2}S_{\mu,1}^\dagger S_{\mu,1} - \frac{iN\gamma}{2}S_{\text{opt},1}^\dagger S_{\text{opt},1}, \end{aligned} \tag{B3}$$

where $S_s^\dagger S_{s'} \coloneqq \sum_{i=1}^N S_{s,i}^\dagger S_{s',i}$ for $s, s' \in \{\mu, \text{opt}\}$. It can be seen from Eq. B3 that the effective Hamiltonian is diagonal in the basis $\mathcal{B}$

$$\mathcal{B} = \{S_{+,1}^\dagger|G\rangle, S_{-,1}^\dagger|G\rangle, \ldots, S_{+,N}^\dagger|G\rangle, S_{-,N}^\dagger|G\rangle\} \tag{B4}$$

where $S_{+,i}^\dagger = \left(S_{\mu,i}^\dagger + S_{\text{opt},i}^\dagger\right)/\sqrt{2}$, and $S_{-,i}^\dagger = \left(S_{\mu,i}^\dagger - S_{\text{opt},i}^\dagger\right)/\sqrt{2}$. It is apparent that, in the diagonal basis, there are only two bright states $\{S_{+,1}^\dagger|G\rangle, S_{-,1}^\dagger|G\rangle\}$; the other states don't couple to the waveguides due to orthogonality. The

effective coupling rates of the bright states are enhanced by N times to $N\gamma_\mu$ and $N\gamma_{\text{opt}}$, hence, the cooperativities are enhanced by N times too. As the effective cooperativity scales linearly with the size of the ensemble, the maximum possible transduction efficiency should increase concurrently. For ensembles that are large enough, the maximum possible transduction efficiency should saturate to unity.

In the presence of inhomogeneous broadening, the advantage from scaling the number of emitters vanishes. The basis $\mathcal{B}$ identified earlier is no longer the diagonal basis for the effective Hamiltonian and the argument that we made in the case of a homogeneous ensemble that led to the scaling of the effective cooperativity can no longer be made. The collective action of the emitters, i.e., superradiance, is hampered by the differences in the emitters. In fact, with increasing inhomogeneous broadening, the maximum possible transmission drops to values corresponding to only a single emitter.

Appendix C: Maximising transduction efficiency through a homogeneous ensemble

For a homogeneous ensemble, as there are only two bright states $\{S^\dagger_{+,1}|G\rangle, S^\dagger_{-,1}|G\rangle\}$ that couple to the waveguides, the ensemble can be equivalently considered to be a single emitter system with the coupling rates to the waveguides enhanced by N. The effective Hamiltonian of the equivalent single-emitter system is,

$$H_{\text{eq}} = \left(\delta_\mu - \frac{i(\Gamma + N\gamma)}{2}\right) S^\dagger_{\mu,1} S_{\mu,1} + \left(\delta_{\text{opt}} - \frac{i(\Gamma + N\gamma)}{2}\right) S^\dagger_{\text{opt},1} S_{\text{opt},1} + \Omega(S^\dagger_{\mu,1} S_{\text{opt},1} + \text{H. c.}). \tag{C1}$$

The transduction spectrum $\tau(\omega)$ through this system is given by [98],

$$\tau(\omega) = \sum_{s\in\{+,-\}} \frac{\langle G|L_{\text{opt}} S^\dagger_{s,1}|G\rangle\langle G|S_{s,1} L^\dagger_\mu|G\rangle}{\omega - E_{s,1}} \tag{C2}$$

where $E_{\pm,1}$ are the eigenvalues of H_{eq}. Assuming $\delta_\mu = \delta_{\text{opt}} = 0$, Eq. C2 leads to,

$$|\tau(\omega)| = \frac{N\gamma\Omega}{|(\omega - E_{+,1})(\omega - E_{-,1})|} \tag{C3}$$

where $E_{\pm,i} = \left(-\frac{i(\Gamma+N\gamma)}{2} \pm \Omega\right)$. For $|\Omega| \leq (N\gamma + \Gamma)/2$, $|\tau(\omega)|$ peaks at $\omega = 0$, with

$$|\tau(0)| = \frac{N\gamma\Omega}{\Omega^2 + \left(\frac{N\gamma+\Gamma}{2}\right)^2}. \tag{C4}$$

Hence, $|\tau(0)|$ is maximized when $\Omega = (N\gamma + \Gamma)/2$ and in that case, $|\tau(0)| = \frac{N\gamma}{\Gamma+N\gamma}$. We point out that when $|\Omega| \gg (N\gamma + \Gamma)/2$, the transduction spectrum has two peaks at $\approx \pm\Omega$, with $|\tau(\pm\Omega)| = \frac{N\gamma}{\Gamma+N\gamma}$. As high drive strengths can be experimentally undesirable, we use the constant drive of least strength that maximises the transduction efficiency, i.e., $\Omega = (N\gamma + \Gamma)/2$, as the benchmark against which the optimized drives are judged.

Appendix D: Hybridisation of eigenstates of a homogeneous ensemble with the introduction of inhomogeneity

Consider the following separation of the effective Hamiltonian of an inhomogeneous ensemble into a Hamiltonian representing a homogeneous ensemble (H_0) and a perturbation term representing the inhomogeneity (V),

$$H_{\text{eff}} = H_0 + \lambda V \tag{D1}$$

$$H_0 = \sum_i \left[-\frac{i\Gamma}{2}\sigma^{i\dagger}_\mu \sigma^i_\mu - \frac{i\Gamma}{2}\sigma^{i\dagger}_{\text{opt}}\sigma^i_{\text{opt}}\right] + \sum_i \Omega(\sigma^{i\dagger}_\mu \sigma^i_{\text{opt}} + \text{H. c.}) - \frac{i}{2}L^\dagger_\mu L_\mu - \frac{i}{2}L^\dagger_{\text{opt}} L_{\text{opt}} \tag{D2}$$

$$V = \sum_i \left[\delta^i_\mu \sigma^{i\dagger}_\mu \sigma^i_\mu + \delta^i_{\text{opt}}\sigma^{i\dagger}_{\text{opt}}\sigma^i_{\text{opt}}\right]. \tag{D3}$$

Defining, $|E_{\pm,i}\rangle = S^\dagger_{\pm,i}|G\rangle$, the eigenstates and eigenvalues of H_0 are,

$$H_0|E_{\pm,1}\rangle = \left(-\frac{i(\Gamma+N\gamma)}{2} \pm \Omega\right)|E_{\pm,1}\rangle \tag{D4}$$

$$H_0|E_{\pm,i}\rangle = \left(-\frac{i\Gamma}{2} \pm \Omega\right)|E_{\pm,i}\rangle,\ i \neq 1 \tag{D5}$$

$$\tag{D6}$$

With the introduction of the perturbation, the first order correction to the eigenstate $|E_{+,(1)}\rangle$ is,

$$|E_{+,1}\rangle \to |E_{+,i}\rangle + \lambda \sum_{\substack{i\neq 1,\\ s\in\{+,-\}}} |E_{s,i}\rangle \frac{\langle E_{s,i}|V|E_{+,1}\rangle}{E_{s,i}-E_{+,1}} + \lambda|E_{-,1}\rangle \frac{\langle E_{-,1}|V|E_{+,1}\rangle}{E_{-,1}-E_{+,1}}. \tag{D7}$$

The second term in Eq. D7 evaluates to zero and,

$$V|E_{+,1}\rangle = \frac{\left(\delta^1_\mu + \delta^1_{\text{opt}}\right)}{2}|E_{+,1}\rangle + \frac{\left(\delta^1_\mu - \delta^1_{\text{opt}}\right)}{2}|E_{-,1}\rangle. \tag{D8}$$

Thus, the perturbation changes the eigenstate as,

$$|E_{+,1}\rangle \to |E_{+,1}\rangle - \frac{\lambda(\delta^1_\mu - \delta^1_{\text{opt}})}{4\Omega}|E_{-,1}\rangle. \tag{D9}$$

This indicates that the relevant frequency scale to compare the inhomogenous broadening to is the drive strength Ω, which explains the variation of the superradiance metric with cooperativity in the unoptimized case in Fig. 4a. The unoptimized drive strength is chosen to be $\Omega(t) = (N\gamma + \Gamma)/2$ and as cooperativity is reduced by increasing Γ, the unoptimized drive strength increases, whereas the inhomogeneous broadening remains constant. Consequently, the hybridisation of the eigenstates away from that of a homogeneous ensemble decreases and the superradiance metric is higher on average.

Appendix E: Efficient calculation of gradients with the time-domain adjoint variable method

In this appendix, we describe how the adjoint variable method can be used to calculate the gradient with respect to all the parameters describing the laser drive efficiently in only two simulations (named forward and backward simulations).

First, we rewrite Eq. A13 and Eq. A10 as,

$$i\frac{dy(t)}{dt} = (H_0 + \Omega(t)H_1)y(t) + v_\mu a_\mu(t) \tag{E1}$$

$$a_{\text{opt}}(t) = v^\dagger_{opt} y(t), \tag{E2}$$

where $y(t) \coloneqq |\psi(t)\rangle$ is the vector describing the state of the ensemble, and

$$H_0 \coloneqq \sum_i \left[\delta^i_\mu \sigma^{i\dagger}_\mu \sigma^i_\mu + \delta^i_{\text{opt}} \sigma^{i\dagger}_{\text{opt}} \sigma^i_{\text{opt}}\right] - \sum_i \left(\frac{i\Gamma_\mu}{2}\sigma^{i\dagger}_\mu \sigma^i_\mu - \frac{i\Gamma_{\text{opt}}}{2}\sigma^{i\dagger}_{\text{opt}}\sigma^i_{\text{opt}}\right) - \frac{i}{2}L^\dagger_\mu L_\mu - \frac{i}{2}L^\dagger_{\text{opt}}L_{\text{opt}} \tag{E3}$$

$$H_1 \coloneqq \sum_i (\sigma^{i\dagger}_\mu \sigma^i_{\text{opt}} + \text{H. c.}) \tag{E4}$$

$$v_\mu \coloneqq L^\dagger_\mu|G\rangle,\ v_{\text{opt}} \coloneqq iL^\dagger_{\text{opt}}|G\rangle \tag{E5}$$

We discretize the total simulation time range $[0, T]$ into $N-1$ steps of duration δt each. On this grid, the differential equation Eq. E1 can be discretized as,

$$y[k+1] = U[k]\left(y[k] - i\delta t\ a_\mu[k]\ v_\mu\right) \qquad k \in \{0, \ldots, N-2\} \tag{E6}$$

$$y[0] = 0 \text{ (initial condition)}, \tag{E7}$$

where, $U[k] \coloneqq \exp\left(-i\ \delta t\left(H_0 + \Omega[k]H_1\right)\right)$, $\Omega[k] \coloneqq \Omega(k\delta t)$, $y[k] \coloneqq y(k\delta t)$, $a_\mu[k] \coloneqq a_\mu(k\delta t)$. We refer to solving this system of equations as the forward simulation.

The transduced power in the optical mode can be expressed in terms of the result of the forward simulation as,

$$P = \sum_{k=0}^{N-1} |a_{\text{opt}}[k]|^2 = \sum_{k=1}^{N-1} |v_{\text{opt}}^\dagger y[k]|^2. \tag{E8}$$

The latter sum starts from $k = 1$ as $y[0] = 0$ is enforced as the initial condition.

The derivative of P with respect to the drive at the lth time step is,

$$\frac{\partial P}{\partial \Omega[l]} = \sum_{k=1}^{N-1} r[k]^\dagger \frac{\partial y[k]}{\partial \Omega[l]} + C.c., \tag{E9}$$

where, '$C.c.$' means 'complex conjugate' and $r[k] \coloneqq \left(v_{\text{opt}}^\dagger y[k]\right)^* v_{\text{opt}}$.

We construct the following block vectors and matrices,

$$y \coloneqq \begin{pmatrix} y[1] \\ y[2] \\ \vdots \\ y[N-1] \end{pmatrix} \quad r \coloneqq \begin{pmatrix} r[1] \\ r[2] \\ \vdots \\ r[N-1] \end{pmatrix} \quad a \coloneqq -i\ \delta t \begin{pmatrix} a_\mu[1] v_\mu \\ a_\mu[2] v_\mu \\ \vdots \\ a_\mu[N-1] v_\mu \end{pmatrix} \tag{E10}$$

$$M \coloneqq \begin{pmatrix} 0 & \cdots & & 0 \\ U[1] & & & \\ & U[2] & & \vdots \\ \vdots & & \ddots & \\ 0 & \cdots & U[N-2] & 0 \end{pmatrix} \quad U \coloneqq \begin{pmatrix} U[0] & 0 & \cdots & 0 \\ 0 & U[1] & \cdots & 0 \\ \vdots & \vdots & \ddots & \vdots \\ 0 & 0 & \cdots & U[N-2] \end{pmatrix}. \tag{E11}$$

The only non-zero blocks in the matrix M are the subdiagonal blocks.

The forward simulation Eq. E6 can now be written as,

$$y = My + Ua \tag{E12}$$

As $\frac{\partial U[k]}{\partial \Omega[l]} = 0$ if $k \neq l$, taking the derivative of Eq. E12 with respect to the drive at the lth time step results in,

$$\frac{\partial y}{\partial \Omega[l]} = M \frac{\partial y}{\partial \Omega[l]} + p[l] \tag{E13}$$

$$\Rightarrow \frac{\partial y}{\partial \Omega[l]} = (\mathbb{1} - M)^{-1} p[l] \qquad l \in \{0, \ldots, N-2\} \tag{E14}$$

where $\mathbb{1}$ is the identity matrix and,

$$p[l] = \begin{pmatrix} 0_{ld \times 1} \\ \alpha[l] \\ 0_{(N-l-2)d \times 1} \end{pmatrix} \tag{E15}$$

$$\alpha[l] = \frac{\partial U[l]}{\partial \Omega[l]} (y[l] + \delta t\ a_\mu[l]\ v_\mu). \tag{E16}$$

In Eq. E15, d is the dimension of the state vector $y(t)$ and $0_{m \times n}$ is a zero matrix of dimension $m \times n$. To calculate $\alpha[l]$, we estimate the derivative $\frac{\partial U[l]}{\partial \Omega[l]}$ by a finite difference.

Using Eq. E14 in Eq. E9, we have,

$$\frac{\partial P}{\partial \Omega[l]} = r^\dagger (\mathbb{1} - M)^{-1} p[l] + C.c. \tag{E17}$$

We define a vector $q = \left(q[1],\ q[2],\ \ldots,\ q[N-1]\right)^T$ such that,

$$q^\dagger \coloneqq r^\dagger (\mathbb{1} - M)^{-1} \tag{E18}$$

$$\Rightarrow q = M^\dagger q + r \tag{E19}$$

Using the definition of M and expanding out Eq. E19 in terms of the elements of q and r results in the following system of equations,

$$q[N-k] = U[N-k]^\dagger q[N-k+1] + r[N-k] \qquad k \in \{2,3,\ldots,N-1\} \tag{E20}$$
$$q[N-1] = r[N-1]. \tag{E21}$$

We refer to $q[k]$ as the adjoint variables and to solving this system of equations (Eq. E20 and Eq. E21) as the backward simulation. The initial condition for the backward simulation is provided at the final time point unlike the forward simulation.

Once the forward and backward simulations are done, the gradient with respect to the drive at each time step can be computed just with an inner product of two $d-$dimensional vectors,

$$\frac{\partial P}{\partial \Omega[l]} = q^\dagger p[l] + C.c., \tag{E22}$$
$$\Rightarrow \frac{\partial P}{\partial \Omega[l]} = q[l+1]^\dagger \alpha[l] + C.c. \tag{E23}$$

The chain rule can then be used to compute the gradient with respect to the harmonic parameters Ω_n and ϕ_n,

$$\frac{\partial P}{\partial \Omega_n} = \sum_{l=0}^{N-2} \frac{\partial \Omega[l]}{\partial \Omega_n}\frac{\partial P}{\partial \Omega[l]} = \sum_{l=0}^{N-2} \cos\left(n\omega_0 l\delta t + \phi_n\right)\frac{\partial P}{\partial \Omega[l]} \tag{E24}$$

$$\frac{\partial P}{\partial \phi_n} = \sum_{l=0}^{N-2} \frac{\partial \Omega[l]}{\partial \phi_n}\frac{\partial P}{\partial \Omega[l]} = \sum_{l=0}^{N-2} -\Omega_n \sin\left(n\omega_0 l\delta t + \phi_n\right)\frac{\partial P}{\partial \Omega[l]} \tag{E25}$$

Appendix F: Derivation of Lagrange duals of problems (2, 6), and upper bound on the optimal value of problem (7)

In this appendix, we show that the Lagrange dual for optimization problem (2) leads to a trivial bound, then we derive the Lagrange dual for the distance-constrained problem (6), and finally provide a derivation for the upper bound ε_c on the optimal value of problem (7).

For notational clarity, we rewrite problem (2) in the following manner,

$$\max_{\Omega(t),y(t)} \quad \int_{-\infty}^{\infty} y(t)^\dagger v_{\text{opt}} v_{\text{opt}}^\dagger y(t)\, dt \tag{F1}$$
$$\text{subject to} \quad \frac{dy(t)}{dt} = -i(H_0 + \Omega(t)H_1)y(t) - iv_\mu a_\mu(t), \tag{F2}$$

where $y(t) \coloneqq |\psi_{\text{e}}(t)\rangle$ and $H_0, H_1, v_\mu, v_{\text{opt}}$ are defined in Eqs. E3, E4, E5.

1. Lagrange dual for problem (2)

Introducing the dual variables $\eta(t)$, the Lagrangian for problem (2) is:

$$\mathcal{L}(y(t),\Omega(t);\eta(t)) = \int_{-\infty}^{\infty} y(t)^\dagger V y(t)\, dt + 2\int_{-\infty}^{\infty} \text{Re}\left[\eta(t)^\dagger\left(\frac{dy(t)}{dt} + iH_1\Omega(t)y(t) + iH_0 y(t) + iv_\mu a_\mu(t)\right)\right], \tag{F3}$$

where Re[.] denotes the real part of a complex number and $V \coloneqq v_{\text{opt}} v_{\text{opt}}^\dagger$. We point out that V is a positive-definite matrix.

Integrating by parts the term with the derivative of the state in the equation above, we have,

$$\mathcal{L}(y(t),\Omega(t);\eta(t)) = \int_{-\infty}^{\infty} y(t)^\dagger V y(t)\, dt + \lim_{T\to\infty} 2\,\text{Re}\left[\eta(T)^\dagger y(T) - \eta(-T)^\dagger y(-T)\right] + \tag{F4}$$
$$\int_{-\infty}^{\infty} 2\,\text{Re}\left[z(t)^\dagger y(t)\right]\, dt + \int_{-\infty}^{\infty} 2\,\text{Re}\left[i\ \eta(t)^\dagger v_\mu a_\mu(t)\right], \tag{F5}$$

where

$$z(t) \coloneqq -\frac{d\eta(t)}{dt} - iH_1\Omega(t)\eta(t) - iH_0\eta(t). \tag{F6}$$

The Lagrange dual function $g\left(\eta\left(t\right)\right)$ is given by,

$$g(\eta(t)) \coloneqq \sup_{y(t),\Omega(t)} \mathcal{L}(y(t),\Omega(t);\eta(t)), \tag{F7}$$

where sup denotes the supremum. As the matrix V is positive-definite, the supremum of the Lagrangian over $y\left(t\right)$ is unbounded as the norm of $y\left(t\right)$ increases, and hence the dual function is unbounded too. Therefore, in this case, Lagrangian duality reveals a trivial upper bound on the transduced power.

2. Lagrange dual for problem (6)

The Lagrangian for problem (6) is

$$\mathcal{L}(y(t);\lambda) = \int_{-\infty}^{\infty} y(t)^\dagger V y(t)\ dt + \lambda\left(\varepsilon - \int_{-\infty}^{\infty} \|y(t) - y_0(t)\|_2^2\ dt\right) \tag{F8}$$

$$= \int_{-\infty}^{\infty} y(t)^\dagger\left(V - \lambda\mathbb{1}\right) y(t)\ dt + \lambda\left(\varepsilon - \int_{-\infty}^{\infty} \|y_0(t)\|_2^2\ dt\right) + \int_{-\infty}^{\infty} 2\,\mathrm{Re}\left[z(t)^\dagger y(t)\right]\ dt \tag{F9}$$

where $y_0\left(t\right) \coloneqq |\psi_{\mathrm{e},0}\left(t\right)\rangle$ is the reference state, λ is a dual variable and $z\left(t\right) \coloneqq \lambda y_0\left(t\right)$. The corresponding dual function is,

$$g(\lambda) = \sup_{y(t)} \mathcal{L}(y(t);\lambda) \tag{F10}$$

$$= \begin{cases} \int_{-\infty}^{\infty} z(t)^\dagger\left(\lambda\mathbb{1} - V\right)^{-1} z(t)\ dt + \lambda\left(\varepsilon - \int_{-\infty}^{\infty} \|y_0(t)\|_2^2\ dt\right), & \text{if } \lambda\mathbb{1} - V \geq 0 \\ \infty, & \text{otherwise} \end{cases} \tag{F11}$$

To obtain the least upper bound, the dual function has to be minimized, leading to the following Lagrange dual problem,

$$\begin{aligned} \min_{\lambda,\beta(t)} \quad & \int_{-\infty}^{\infty} \beta(t)\ dt + \lambda\left(\varepsilon - \int_{-\infty}^{\infty} \|y_0(t)\|_2^2\ dt\right) \\ \text{subject to} \quad & \beta(t) \geq z(t)^\dagger(\lambda\mathbb{1} - V)^{-1} z(t) \\ & \lambda\mathbb{1} - V \geq 0, \end{aligned}$$

where we have introduced additional dual variables $\beta\left(t\right)$.

3. Upper bound on ε^*

Eq. E1 can further be rewritten as,

$$\frac{dy(t)}{dt} = (-iH_{\mathrm{sys}}(\Omega(t)) - D)y(t) - iv_\mu a_\mu(t) \tag{F12}$$

where $H_{\mathrm{sys}}\left(\Omega\left(t\right)\right)$ is defined in Eq. A1 and,

$$D \coloneqq \sum_i \left(\frac{\Gamma_\mu}{2}\sigma_\mu^{i\dagger}\sigma_\mu^i + \frac{\Gamma_{\mathrm{opt}}}{2}\sigma_{\mathrm{opt}}^{i\dagger}\sigma_{\mathrm{opt}}^i\right) + \frac{1}{2}L_\mu^\dagger L_\mu + \frac{1}{2}L_{\mathrm{opt}}^\dagger L_{\mathrm{opt}}. \tag{F13}$$

Using the fact that $D^\dagger = D$, the time-evolution of the norm of the state can be written as,

$$\frac{dy(t)^\dagger y(t)}{dt} = -2y(t)^\dagger D y(t) + 2\,\mathrm{Re}\left[-iy(t)^\dagger v_\mu a_\mu(t)\right] \tag{F14}$$

$$\leq -2d_{\min} y(t)^\dagger y(t) + 2\,\mathrm{Re}\left[-iy(t)^\dagger v_\mu a_\mu(t)\right], \tag{F15}$$

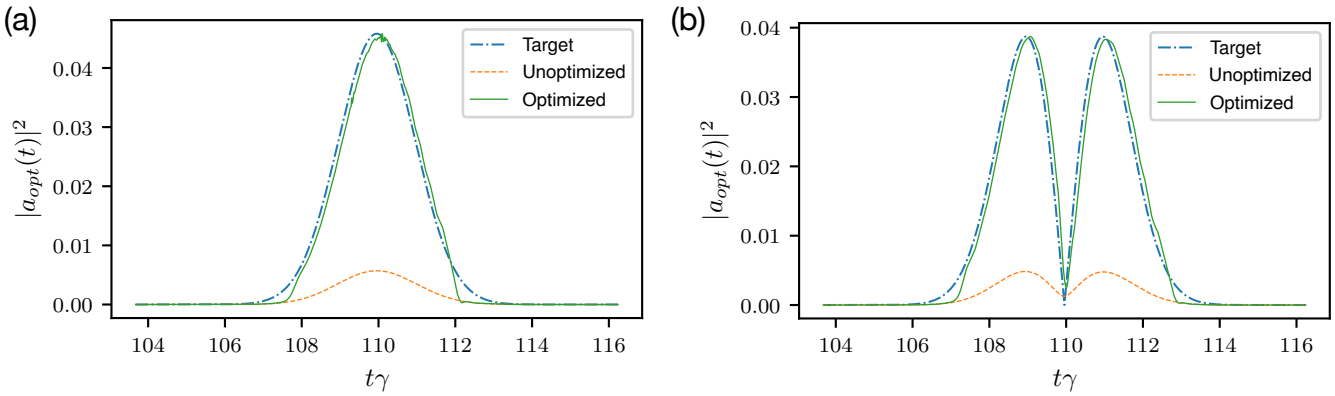

Figure 7. Temporal mode overlap-based design of drives. The amplitude $|a_{\text{opt}}(t)|^2$ of the output photon's temporal wave-packet after transduction by an ensemble of emitters with $N = 10$, $C = 0.1$, $\Delta \approx 61.61\gamma$, and under the application of drives obtained by locally solving problem (G1) for (a) $n = 0$, $a_\mu(t) = \varphi_0(t)$ and (b) $n = 1$, $a_\mu(t) = \varphi_1(t)$. The curves labelled 'Target' represent the (amplitude of the) Hermite-Gaussian modes $\varphi_0(t), \varphi_1(t)$, respectively. The improvement in the transduced output power in the desired target modes are (a) $\approx 61.05\times$ and (b) $\approx 62.43\times$. The ratio of the output power in the target mode to the total output power are (a) $\approx 99\%$ and (b) $\approx 98.6\%$. The input photon's central frequency is fixed at the resonance of a homogeneous ensemble for both cases.

where $d_{\min}$ is the smallest eigenvalue of D.

From the inequality (F15) we have,

$$\|y(t)\|_2^2 \leq \int_0^t e^{-2d_{\min}(t-\tau)} 2\,\text{Re}\left[-iy(\tau)^\dagger v_\mu a_\mu(\tau)\right]\, d\tau \tag{F16}$$

$$\leq \int_0^t 2e^{-2d_{\min}(t-\tau)} \|y(\tau)\|_2 \|v_\mu a_\mu(\tau)\|_2\, d\tau \tag{F17}$$

$$\leq \int_0^t 2e^{-2d_{\min}(t-\tau)} \|v_\mu a_\mu(\tau)\|_2\, d\tau := d(t), \tag{F18}$$

where, to go from (F17) to (F18) we use the fact $\|y(t)\|_2 \leq 1,\ \forall t$.

Therefore,

$$\int_{-\infty}^{\infty} \|y(t) - y_0(t)\|_2^2\, dt \leq \int_{-\infty}^{\infty} \left(\|y(t)\|_2 + \|y_0(t)\|_2\right)^2\, dt \tag{F19}$$

$$\leq \int_{-\infty}^{\infty} \left(\sqrt{d(t)} + \|y_0(t)\|_2\right)^2\, dt := \varepsilon_c \tag{F20}$$

Appendix G: Design of optimized drives with overlap-based objectives

Quantum information can be encoded in the temporal modes of photons for the purposes of quantum communication [112]. Such encoding would necessitate a transduction process that preserves the fidelity of the transduced photon's wave-packet to specific temporal modes. We demonstrate in this appendix that it is possible to extend our design method to compensate for inhomogeneous broadening and produce improvements in transduction efficiency while preserving the overlap with a specified temporal mode.

To achieve this, we pose the design of the drive as maximising the overlap of the output photon's temporal wave-packet with a specified Hermite-Gaussian function [113]. For example,

$$\max_{\Omega(t)} \quad \left|\int_{-\infty}^{\infty} dt\ \varphi_n(t) a_{\text{opt}}(t)\right|^2 \tag{G1}$$

$$\text{subject to} \quad i\frac{d|\psi_e(t)\rangle}{dt} = H_{\text{eff}}(\Omega(t))\,|\psi_e(t)\rangle + a_\mu(t) L_\mu^\dagger |G\rangle, \tag{G2}$$

$$a_{\text{opt}}(t) = -i\langle G|L_{\text{opt}}|\psi_e(t)\rangle. \tag{G3}$$

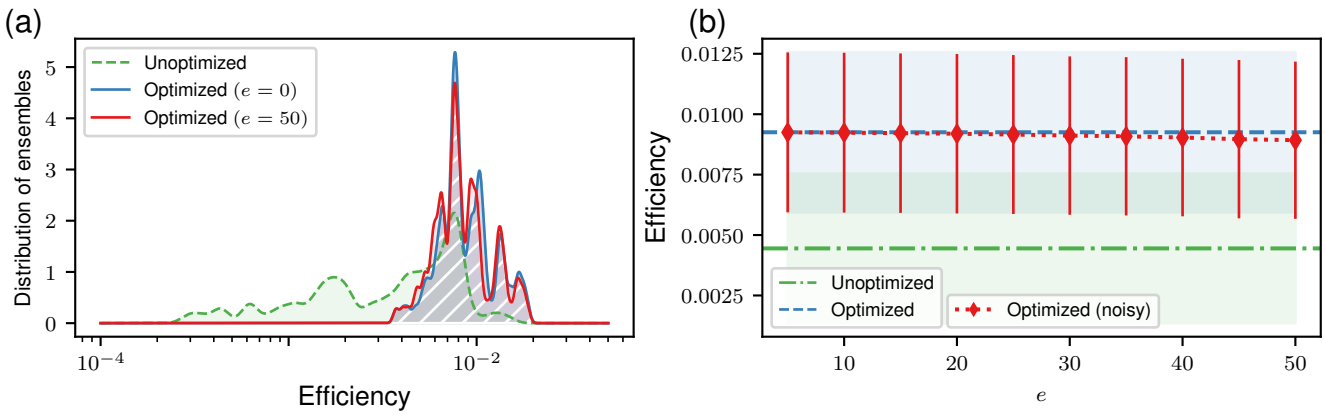

Figure 8. Effect of noise on optimized drives. (a) Density plots (obtained by kernel density estimation using Gaussian kernels [104]) of the transduction efficiency through 100 ensembles with inhomogeneous broadening $\Delta = 200\gamma$, $C = 0.1$ for three cases – (green) no optimized drive is applied, (blue) optimized drives (custom-designed for each of the 100 random ensembles) are applied, (red) noise ($e = 50$) is added to the customized optimized drives. For all cases, the input-photon is frequency-shifted to match the highest peak of the unoptimized transmission spectrum. (b) Statistics of the transduction efficiency with increasing noise percentage (e) in the optimized drive compared with the noiseless optimized and unoptimized cases. Lines denote the mean of the transduction efficiency over 100 ensembles and the shaded areas and error bars denote the standard deviation.

where $\varphi_n(t)$ is the nth-order Hermite-Gaussian function (normalized to unity) [113] — if the input microwave photon occupies the nth-order Hermite-Gaussian mode, i.e. $a_\mu(t) = \varphi_n(t)$, we solve G1 to design a drive such that the output optical photon's power is concentrated in the nth-order mode too. We solve problem (G1) for a randomly generated inhomogeneous ensemble with $N = 10$ emitters and input microwave photons occupying the 0th- and 1st-order Hermite Gaussian modes ($n = 0, 1$). Fig. 7 shows that we observe improved transduction efficiencies into the desired output target mode in both cases. Furthermore, the ratio of the power in the desired output target mode to the total transduced output power is close to 99% in both cases.

Appendix H: Effect of noise in optimized drives

Experimental realizations (through laser pulse shaping) of the optimized drives generated by our design procedure will be subject to random noise in the form of intensity fluctuations. In this appendix, we analyze the effect of noise on the performance of optimized drives. For a time-dependent optimized drive $\Omega(t)$, we consider multiplicative noise of the following form,

$$\Omega_{\text{noisy}}(t) = \Omega(t)\,(1 + E_t/100)\,, \tag{H1}$$

where E_t are independent and identically distributed random variables with the following (uniform) probability densities parametrized by a variable e,

$$p_{E_t}(x) = \begin{cases} \frac{1}{2e} & \text{if } x \in [-e, e] \\ 0, & \text{otherwise} \end{cases}. \tag{H2}$$

We apply the noise described above to customized optimized drives designed for 100 randomly inhomogeneously broadened ensembles of size $N = 10$ and $\Delta = 200\gamma$. Fig. 8 shows that even as the noise percentage parameter e is increased up to 50, the performance of the optimized drive decreases only slightly.

[1] Frank Arute, Kunal Arya, Ryan Babbush, Dave Bacon, *et al.*, "Quantum supremacy using a programmable superconducting processor," Nature **574**, 505–510 (2019).

[2] H. J. Kimble, "The quantum internet," Nature **453**, 1023–1030 (2008).
[3] Paul Magnard, Simon Storz, Philipp Kurpiers, Josua Schär, *et al.*, "Microwave Quantum Link between Superconducting Circuits Housed in Spatially Separated Cryogenic Systems," arXiv:2008.01642 [quant-ph] (2020), arXiv:2008.01642 [quant-ph].
[4] Nicholas J. Lambert, Alfredo Rueda, Florian Sedlmeir, and Harald G. L. Schwefel, "Coherent Conversion Between Microwave and Optical Photons—An Overview of Physical Implementations," Advanced Quantum Technologies **3**, 1900077 (2020).
[5] Nikolai Lauk, Neil Sinclair, Shabir Barzanjeh, Jacob P. Covey, Mark Saffman, Maria Spiropulu, and Christoph Simon, "Perspectives on quantum transduction," Quantum Science and Technology **5**, 020501 (2020).
[6] Timothy P. McKenna, Jeremy D. Witmer, Rishi N. Patel, Wentao Jiang, *et al.*, "Cryogenic microwave-to-optical conversion using a triply-resonant lithium niobate on sapphire transducer," arXiv:2005.00897 [physics, physics:quant-ph] (2020), arXiv:2005.00897 [physics, physics:quant-ph].
[7] Jeffrey Holzgrafe, Neil Sinclair, Di Zhu, Amirhassan Shams-Ansari, *et al.*, "Cavity electro-optics in thin-film lithium niobate for efficient microwave-to-optical transduction," arXiv:2005.00939 [physics, physics:quant-ph] (2020), arXiv:2005.00939 [physics, physics:quant-ph].
[8] Mohammad Soltani, Mian Zhang, Colm Ryan, Guilhem J. Ribeill, Cheng Wang, and Marko Loncar, "Efficient quantum microwave-to-optical conversion using electro-optic nanophotonic coupled resonators," Physical Review A **96**, 043808 (2017).
[9] Mankei Tsang, "Cavity quantum electro-optics," Physical Review A **81**, 063837 (2010).
[10] Alfredo Rueda, William Hease, Shabir Barzanjeh, and Johannes M. Fink, "Electro-optic entanglement source for microwave to telecom quantum state transfer," npj Quantum Information **5**, 1–11 (2019).
[11] Alfredo Rueda, Florian Sedlmeir, Michele C. Collodo, Ulrich Vogl, *et al.*, "Efficient microwave to optical photon conversion: An electro-optical realization," Optica **3**, 597–604 (2016).
[12] R. Hisatomi, A. Osada, Y. Tabuchi, T. Ishikawa, *et al.*, "Bidirectional conversion between microwave and light via ferromagnetic magnons," Physical Review B **93**, 174427 (2016).
[13] Jonathan R. Everts, Matthew C. Berrington, Rose L. Ahlefeldt, and Jevon J. Longdell, "Microwave to optical photon conversion via fully concentrated rare-earth-ion crystals," Physical Review A **99**, 063830 (2019).
[14] Jonathan Everts, Gavin G. G. King, Nicholas Lambert, Sacha Kocsis, Sven Rogge, and Jevon J. Longdell, "Ultrastrong coupling between a microwave resonator and antiferromagnetic resonances of rare earth ion spins," Physical Review B **101**, 214414 (2020), arXiv:1911.11311.
[15] Changchun Zhong, Zhixin Wang, Changling Zou, Mengzhen Zhang, *et al.*, "Proposal for Heralded Generation and Detection of Entangled Microwave–Optical-Photon Pairs," Physical Review Letters **124**, 010511 (2020).
[16] Marcelo Wu, Emil Zeuthen, Krishna Coimbatore Balram, and Kartik Srinivasan, "Microwave-to-Optical Transduction Using a Mechanical Supermode for Coupling Piezoelectric and Optomechanical Resonators," Physical Review Applied **13**, 014027 (2020).
[17] Hoi-Kwan Lau and Aashish A. Clerk, "Ground state cooling and high-fidelity quantum transduction via parametrically-driven bad-cavity optomechanics," Physical Review Letters **124**, 103602 (2020), arXiv:1904.12984.
[18] Wentao Jiang, Christopher J. Sarabalis, Yanni D. Dahmani, Rishi N. Patel, *et al.*, "Efficient bidirectional piezo-optomechanical transduction between microwave and optical frequency," Nature Communications **11**, 1–7 (2020).
[19] Moritz Forsch, Robert Stockill, Andreas Wallucks, Igor Marinković, *et al.*, "Microwave-to-optics conversion using a mechanical oscillator in its quantum ground state," Nature Physics **16**, 69–74 (2020).
[20] G. Arnold, M. Wulf, S. Barzanjeh, E. S. Redchenko, *et al.*, "Converting microwave and telecom photons with a silicon photonic nanomechanical interface," Nature Communications **11**, 4460 (2020).
[21] T. Bagci, A. Simonsen, S. Schmid, L. G. Villanueva, *et al.*, "Optical detection of radio waves through a nanomechanical transducer," Nature **507**, 81–85 (2014).
[22] R. W. Andrews, R. W. Peterson, T. P. Purdy, K. Cicak, R. W. Simmonds, C. A. Regal, and K. W. Lehnert, "Bidirectional and efficient conversion between microwave and optical light," Nature Physics **10**, 321–326 (2014).
[23] Ying-Dan Wang and Aashish A. Clerk, "Using Interference for High Fidelity Quantum State Transfer in Optomechanics," Physical Review Letters **108**, 153603 (2012).
[24] Lin Tian, "Adiabatic State Conversion and Pulse Transmission in Optomechanical Systems," Physical Review Letters **108**, 153604 (2012).
[25] Jeff T. Hill, Amir H. Safavi-Naeini, Jasper Chan, and Oskar Painter, "Coherent optical wavelength conversion via cavity optomechanics," Nature Communications **3**, 1196 (2012).
[26] Sh. Barzanjeh, M. Abdi, G. J. Milburn, P. Tombesi, and D. Vitali, "Reversible Optical-to-Microwave Quantum Interface," Physical Review Letters **109**, 130503 (2012).
[27] Amir H. Safavi-Naeini and Oskar Painter, "Proposal for an optomechanical traveling wave phonon–photon translator," New Journal of Physics **13**, 013017 (2011).
[28] L. Tian and Hailin Wang, "Optical wavelength conversion of quantum states with optomechanics," Physical Review A **82**, 053806 (2010).
[29] K. Stannigel, P. Rabl, A. S. Sørensen, P. Zoller, and M. D. Lukin, "Optomechanical Transducers for Long-Distance Quantum Communication," Physical Review Letters **105**, 220501 (2010).
[30] John G. Bartholomew, Jake Rochman, Tian Xie, Jonathan M. Kindem, *et al.*, "On-chip coherent microwave-to-optical transduction mediated by ytterbium in YVO$_4$," Nature Communications **11**, 3266 (2020), arXiv:1912.03671.

[31] Peter S. Barnett and Jevon J. Longdell, "Theory of Microwave-Optical Conversion Using Rare-Earth Ion Dopants," arXiv:2008.10834 [quant-ph] (2020), arXiv:2008.10834 [quant-ph].

[32] Sacha Welinski, Philip J. T. Woodburn, Nikolai Lauk, Rufus L. Cone, Christoph Simon, Philippe Goldner, and Charles W. Thiel, "Electron Spin Coherence in Optically Excited States of Rare-Earth Ions for Microwave to Optical Quantum Transducers," Physical Review Letters **122**, 247401 (2019).

[33] Thibault Vogt, Christian Gross, Jingshan Han, Sambit B. Pal, Mark Lam, Martin Kiffner, and Wenhui Li, "Efficient microwave-to-optical conversion using Rydberg atoms," Physical Review A **99**, 023832 (2019).

[34] David Petrosyan, Klaus Mølmer, József Fortágh, and Mark Saffman, "Microwave to optical conversion with atoms on a superconducting chip," New Journal of Physics **21**, 073033 (2019).

[35] Xavier Fernandez-Gonzalvo, Sebastian P. Horvath, Yu-Hui Chen, and Jevon J. Longdell, "Cavity-enhanced Raman heterodyne spectroscopy in $\mathbf{Er^{3+}:Y_2SiO_5}$ for microwave to optical signal conversion," Physical Review A **100**, 033807 (2019).

[36] Jacob P. Covey, Alp Sipahigil, and Mark Saffman, "Microwave-to-optical conversion via four-wave mixing in a cold ytterbium ensemble," Physical Review A **100**, 012307 (2019).

[37] Jingshan Han, Thibault Vogt, Christian Gross, Dieter Jaksch, Martin Kiffner, and Wenhui Li, "Coherent Microwave-to-Optical Conversion via Six-Wave Mixing in Rydberg Atoms," Physical Review Letters **120**, 093201 (2018).

[38] Bryan T. Gard, Kurt Jacobs, R. McDermott, and M. Saffman, "Microwave-to-optical frequency conversion using a cesium atom coupled to a superconducting resonator," Physical Review A **96**, 013833 (2017).

[39] Martin Kiffner, Amir Feizpour, Krzysztof T. Kaczmarek, Dieter Jaksch, and Joshua Nunn, "Two-way interconversion of millimeter-wave and optical fields in Rydberg gases," New Journal of Physics **18**, 093030 (2016).

[40] Xavier Fernandez-Gonzalvo, Yu-Hui Chen, Chunming Yin, Sven Rogge, and Jevon J. Longdell, "Coherent frequency up-conversion of microwaves to the optical telecommunications band in an Er:YSO crystal," Physical Review A **92**, 062313 (2015).

[41] Lewis A. Williamson, Yu-Hui Chen, and Jevon J. Longdell, "Magneto-Optic Modulator with Unit Quantum Efficiency," Physical Review Letters **113**, 203601 (2014).

[42] Christopher O'Brien, Nikolai Lauk, Susanne Blum, Giovanna Morigi, and Michael Fleischhauer, "Interfacing Superconducting Qubits and Telecom Photons via a Rare-Earth-Doped Crystal," Physical Review Letters **113**, 063603 (2014).

[43] M. Hafezi, Z. Kim, S. L. Rolston, L. A. Orozco, B. L. Lev, and J. M. Taylor, "Atomic interface between microwave and optical photons," Physical Review A **85**, 020302 (2012).

[44] J. Verdú, H. Zoubi, Ch. Koller, J. Majer, H. Ritsch, and J. Schmiedmayer, "Strong Magnetic Coupling of an Ultracold Gas to a Superconducting Waveguide Cavity," Physical Review Letters **103**, 043603 (2009).

[45] Atac Imamoğlu, "Cavity QED Based on Collective Magnetic Dipole Coupling: Spin Ensembles as Hybrid Two-Level Systems," Physical Review Letters **102**, 083602 (2009).

[46] Xiaobo Zhu, Shiro Saito, Alexander Kemp, Kosuke Kakuyanagi, *et al.*, "Coherent coupling of a superconducting flux qubit to an electron spin ensemble in diamond," Nature **478**, 221–224 (2011).

[47] Gavin Dold, Christoph W. Zollitsch, James O'Sullivan, Sacha Welinski, *et al.*, "High-Cooperativity Coupling of a Rare-Earth Spin Ensemble to a Superconducting Resonator Using Yttrium Orthosilicate as a Substrate," Physical Review Applied **11**, 054082 (2019).

[48] Constantin Dory, Dries Vercruysse, Ki Youl Yang, Neil V. Sapra, *et al.*, "Inverse-designed diamond photonics," Nature Communications **10**, 3309 (2019).

[49] Daniil M. Lukin, Constantin Dory, Melissa A. Guidry, Ki Youl Yang, *et al.*, "4H-silicon-carbide-on-insulator for integrated quantum and nonlinear photonics," Nature Photonics **14**, 330–334 (2020).

[50] Noel H. Wan, Tsung-Ju Lu, Kevin C. Chen, Michael P. Walsh, *et al.*, "Large-scale integration of artificial atoms in hybrid photonic circuits," Nature **583**, 226–231 (2020).

[51] R. H. Dicke, "Coherence in Spontaneous Radiation Processes," Physical Review **93**, 99–110 (1954).

[52] M. Gross and S. Haroche, "Superradiance: An essay on the theory of collective spontaneous emission," Physics Reports **93**, 301–396 (1982).

[53] Rahul Trivedi, Marina Radulaski, Kevin A. Fischer, Shanhui Fan, and Jelena Vučković, "Photon Blockade in Weakly Driven Cavity Quantum Electrodynamics Systems with Many Emitters," Physical Review Letters **122**, 243602 (2019).

[54] L.-M. Duan, M. D. Lukin, J. I. Cirac, and P. Zoller, "Long-distance quantum communication with atomic ensembles and linear optics," Nature **414**, 413–418 (2001).

[55] A. González-Tudela, V. Paulisch, D. E. Chang, H. J. Kimble, and J. I. Cirac, "Deterministic Generation of Arbitrary Photonic States Assisted by Dissipation," Physical Review Letters **115**, 163603 (2015).

[56] V. Paulisch, M. Perarnau-Llobet, A. González-Tudela, and J. I. Cirac, "Quantum metrology with one-dimensional superradiant photonic states," Physical Review A **99**, 043807 (2019).

[57] Ruffin E. Evans, Alp Sipahigil, Denis D. Sukachev, Alexander S. Zibrov, and Mikhail D. Lukin, "Narrow-Linewidth Homogeneous Optical Emitters in Diamond Nanostructures via Silicon Ion Implantation," Physical Review Applied **5**, 044010 (2016).

[58] A. M. Dibos, M. Raha, C. M. Phenicie, and J. D. Thompson, "Atomic Source of Single Photons in the Telecom Band," Physical Review Letters **120**, 243601 (2018).

[59] Tian Zhong, Jonathan M. Kindem, John G. Bartholomew, Jake Rochman, *et al.*, "Optically Addressing Single Rare-Earth Ions in a Nanophotonic Cavity," Physical Review Letters **121**, 183603 (2018).

[60] D. Dong and I. R. Petersen, "Quantum control theory and applications: A survey," IET Control Theory Applications **4**, 2651–2671 (2010).

[61] Christiane P Koch, "Controlling open quantum systems: Tools, achievements, and limitations," Journal of Physics: Condensed Matter **28**, 213001 (2016).

[62] Nikodem Grzesiak, Reinhold Blümel, Kenneth Wright, Kristin M. Beck, *et al.*, "Efficient arbitrary simultaneously entangling gates on a trapped-ion quantum computer," Nature Communications **11**, 2963 (2020).

[63] Uffe V. Poulsen, Shlomo Sklarz, David Tannor, and Tommaso Calarco, "Correcting errors in a quantum gate with pushed ions via optimal control," Physical Review A **82**, 012339 (2010).

[64] Michael H. Goerz, Eli J. Halperin, Jon M. Aytac, Christiane P. Koch, and K. Birgitta Whaley, "Robustness of high-fidelity Rydberg gates with single-site addressability," Physical Review A **90**, 032329 (2014).

[65] Philipp Treutlein, Theodor W. Hänsch, Jakob Reichel, Antonio Negretti, Markus A. Cirone, and Tommaso Calarco, "Microwave potentials and optimal control for robust quantum gates on an atom chip," Physical Review A **74**, 022312 (2006).

[66] Alexey V. Gorshkov, Tommaso Calarco, Mikhail D. Lukin, and Anders S. Sørensen, "Photon storage in Λ-type optically dense atomic media. IV. Optimal control using gradient ascent," Physical Review A **77**, 043806 (2008).

[67] Michael H. Goerz, Daniel M. Reich, and Christiane P. Koch, "Optimal control theory for a unitary operation under dissipative evolution," New Journal of Physics **16**, 055012 (2014).

[68] M. Werninghaus, D. J. Egger, F. Roy, S. Machnes, F. K. Wilhelm, and S. Filipp, "Leakage reduction in fast superconducting qubit gates via optimal control," npj Quantum Information **7**, 1–6 (2021).

[69] Mohamed Abdelhafez, Brian Baker, András Gyenis, Pranav Mundada, Andrew A. Houck, David Schuster, and Jens Koch, "Universal gates for protected superconducting qubits using optimal control," Physical Review A **101**, 022321 (2020).

[70] Jochen Scheuer, Xi Kong, Ressa S. Said, Jeson Chen, *et al.*, "Precise qubit control beyond the rotating wave approximation," New Journal of Physics **16**, 093022 (2014).

[71] G. Waldherr, Y. Wang, S. Zaiser, M. Jamali, *et al.*, "Quantum error correction in a solid-state hybrid spin register," Nature **506**, 204–207 (2014).

[72] Jr-Shin Li and Navin Khaneja, "Control of inhomogeneous quantum ensembles," Physical Review A **73**, 030302 (2006).

[73] Jr-Shin Li and Navin Khaneja, "Ensemble Control of Bloch Equations," IEEE Transactions on Automatic Control **54**, 528–536 (2009).

[74] Herschel Rabitz and Gabriel Turinici, "Controlling quantum dynamics regardless of laser beam spatial profile and molecular orientation," Physical Review A **75**, 043409 (2007).

[75] Gabriel Turinici and Herschel Rabitz, "Optimally controlling the internal dynamics of a randomly oriented ensemble of molecules," Physical Review A **70**, 063412 (2004).

[76] H K Cummins and J A Jones, "Use of composite rotations to correct systematic errors in NMR quantum computation," New Journal of Physics **2**, 6–6 (2000).

[77] Kenneth R. Brown, Aram W. Harrow, and Isaac L. Chuang, "Arbitrarily accurate composite pulse sequences," Physical Review A **70**, 052318 (2004).

[78] Philip Owrutsky and Navin Khaneja, "Control of inhomogeneous ensembles on the Bloch sphere," Physical Review A **86**, 022315 (2012).

[79] Quentin Ansel, Steffen J. Glaser, and Dominique Sugny, "Selective and robust time-optimal rotations of spin systems," Journal of Physics A: Mathematical and Theoretical **54**, 085204 (2021).

[80] Nicolas Augier, Ugo Boscain, and Mario Sigalotti, "Adiabatic Ensemble Control of a Continuum of Quantum Systems," SIAM Journal on Control and Optimization **56**, 4045–4068 (2018).

[81] R. Tycko, "Broadband Population Inversion," Physical Review Letters **51**, 775–777 (1983).

[82] Malcolm H. Levitt, "Composite pulses," Progress in Nuclear Magnetic Resonance Spectroscopy **18**, 61–122 (1986).

[83] Brian E. Mischuck, Seth T. Merkel, and Ivan H. Deutsch, "Control of inhomogeneous atomic ensembles of hyperfine qudits," Physical Review A **85**, 022302 (2012).

[84] B. Khani, S. T. Merkel, F. Motzoi, Jay M. Gambetta, and F. K. Wilhelm, "High-fidelity quantum gates in the presence of dispersion," Physical Review A **85**, 022306 (2012).

[85] Navin Khaneja, Timo Reiss, Cindie Kehlet, Thomas Schulte-Herbrüggen, and Steffen J. Glaser, "Optimal control of coupled spin dynamics: Design of NMR pulse sequences by gradient ascent algorithms," Journal of Magnetic Resonance **172**, 296–305 (2005).

[86] Justin Ruths and Jr-Shin Li, "A multidimensional pseudospectral method for optimal control of quantum ensembles," The Journal of Chemical Physics **134**, 044128 (2011).

[87] Chunlin Chen, Daoyi Dong, Ruixing Long, Ian R. Petersen, and Herschel A. Rabitz, "Sampling-based learning control of inhomogeneous quantum ensembles," Physical Review A **89**, 023402 (2014).

[88] Jr-Shin Li, Justin Ruths, Tsyr-Yan Yu, Haribabu Arthanari, and Gerhard Wagner, "Optimal pulse design in quantum control: A unified computational method," Proceedings of the National Academy of Sciences **108**, 1879–1884 (2011).

[89] Justin Ruths and Jr-Shin Li, "Optimal Control of Inhomogeneous Ensembles," IEEE Transactions on Automatic Control **57**, 2021–2032 (2012).

[90] Gabriel Turinici, "Stochastic learning control of inhomogeneous quantum ensembles," Physical Review A **100**, 053403 (2019).

[91] Sen Kuang and Xiaoke Guan, "Robustness of continuous non-smooth finite-time Lyapunov control for two-level quantum systems," IET Control Theory & Applications **14**, 2449–2454 (2020).

[92] Re-Bing Wu, Haijin Ding, Daoyi Dong, and Xiaoting Wang, "Learning robust and high-precision quantum controls," Physical Review A **99**, 042327 (2019).

[93] Yingying Sun, Hailan Ma, Chengzhi Wu, Chunlin Chen, and Daoyi Dong, "Ensemble control of open quantum systems using differential evolution," in *2015 10th Asian Control Conference (ASCC)* (2015) pp. 1–6.

[94] Shuo Wang and Jr-Shin Li, "Free-endpoint optimal control of inhomogeneous bilinear ensemble systems," Automatica **95**, 306–315 (2018).

[95] Sen Kuang, Peng Qi, and Shuang Cong, "Approximate time-optimal control of quantum ensembles based on sampling and learning," Physics Letters A **382**, 1858–1863 (2018).

[96] L. Van Damme, Q. Ansel, S. J. Glaser, and D. Sugny, "Robust optimal control of two-level quantum systems," Physical Review A **95**, 063403 (2017).

[97] Ameneh Arjmandzadeh and Majid Yarahmadi, "Quantum Genetic Learning Control of Quantum Ensembles with Hamiltonian Uncertainties," Entropy **19**, 376 (2017).

[98] Rahul Trivedi, Kevin Fischer, Shanshan Xu, Shanhui Fan, and Jelena Vuckovic, "Few-photon scattering and emission from low-dimensional quantum systems," Physical Review B **98**, 144112 (2018).

[99] Rahul Trivedi, Alex White, Shanhui Fan, and Jelena Vučković, "Analytic and geometric properties of scattering from periodically modulated quantum-optical systems," Physical Review A **102**, 033707 (2020).

[100] E. Rephaeli and S. Fan, "Few-Photon Single-Atom Cavity QED With Input-Output Formalism in Fock Space," IEEE Journal of Selected Topics in Quantum Electronics **18**, 1754–1762 (2012).

[101] Shanhui Fan, Şükrü Ekin Kocabaş, and Jung-Tsung Shen, "Input-output formalism for few-photon transport in one-dimensional nanophotonic waveguides coupled to a qubit," Physical Review A **82**, 063821 (2010).

[102] Werner H. Schmidt, "Numerical Methods for Optimal Control Problems with ODE or Integral Equations," in *Large-Scale Scientific Computing*, Lecture Notes in Computer Science, edited by Ivan Lirkov, Svetozar Margenov, and Jerzy Waśniewski (Springer, Berlin, Heidelberg, 2006) pp. 255–262.

[103] Mohamed A. Swillam, Mohamed H. Bakr, and Xun Li, "Accurate sensitivity analysis of photonic devices that exploit the finite-difference time-domain central adjoint variable method," Applied Optics **46**, 1492–1499 (2007).

[104] David W. Scott, *Multivariate Density Estimation*, 1st ed. (John Wiley & Sons, Ltd, 1992).

[105] Stephen Boyd and Lieven Vandenberghe, *Convex Optimization* (Cambridge University Press, Cambridge, 2004).

[106] Rahul Trivedi, Guillermo Angeris, Logan Su, Stephen Boyd, Shanhui Fan, and Jelena Vučković, "Bounds for Scattering from Absorptionless Electromagnetic Structures," Physical Review Applied **14**, 014025 (2020).

[107] Kamanasish Debnath, Yuan Zhang, and Klaus Mølmer, "Collective dynamics of inhomogeneously broadened emitters coupled to an optical cavity with narrow linewidth," Physical Review A **100**, 053821 (2019).

[108] Daniil M. Lukin, Alexander D. White, Rahul Trivedi, Melissa A. Guidry, *et al.*, "Spectrally reconfigurable quantum emitters enabled by optimized fast modulation," npj Quantum Information **6**, 1–9 (2020).

[109] Kevin C. Miao, Alexandre Bourassa, Christopher P. Anderson, Samuel J. Whiteley, *et al.*, "Electrically driven optical interferometry with spins in silicon carbide," Science Advances **5**, eaay0527 (2019).

[110] M. Metcalfe, S. M. Carr, A. Muller, G. S. Solomon, and J. Lawall, "Resolved Sideband Emission of **InAs**/**GaAs** Quantum Dots Strained by Surface Acoustic Waves," Physical Review Letters **105**, 037401 (2010).

[111] Diederik P. Kingma and Jimmy Ba, "Adam: A Method for Stochastic Optimization," arXiv:1412.6980 [cs] (2017), arXiv:1412.6980 [cs].

[112] B. Brecht, Dileep V. Reddy, C. Silberhorn, and M. G. Raymer, "Photon Temporal Modes: A Complete Framework for Quantum Information Science," Physical Review X **5**, 041017 (2015).

[113] R. Courant and D. Hilbert, "Series Expansions of Arbitrary Functions," in *Methods of Mathematical Physics* (John Wiley & Sons, Ltd, 1989) Chap. 2, pp. 48–111.